Check for updates

Redox-Regulated Adaptation of *Streptococcus oligofermentans* to Hydrogen Peroxide Stress

Huichun Tong,[a,b] Yuzhu Dong,[a,b] Xinhui Wang,[a,b] Qingqing Hu,[a,b] Fan Yang,[c] Meiqi Yi,[c] Haiteng Deng,[c] ⬤ Xiuzhu Dong[a,b]

[a]State Key Laboratory of Microbial Resources, Institute of Microbiology, Chinese Academy of Sciences, Beijing, China
[b]University of Chinese Academy of Sciences, Beijing, China
[c]MOE Key Laboratory of Bioinformatics, School of Life Sciences, Tsinghua University, Beijing, China

Huichun Tong, Yuzhu Dong, and Xinhui Wang contributed equally to this article. Author order was determined on the basis of seniority.

ABSTRACT Preexposure to a low concentration of H_2O_2 significantly increases the survivability of catalase-negative streptococci in the presence of a higher concentration of H_2O_2. However, the mechanisms of this adaptation remain unknown. Here, using a redox proteomics assay, we identified 57 and 35 cysteine-oxidized proteins in *Streptococcus oligofermentans* bacteria that were anaerobically cultured and then pulsed with 40 μM H_2O_2 and that were statically grown in a 40-ml culture, respectively. The oxidized proteins included the peroxide-responsive repressor PerR, the manganese uptake repressor MntR, thioredoxin system proteins Trx and Tpx, and most glycolytic proteins. Cysteine oxidations of these proteins were verified through redox Western blotting, immunoprecipitation, and liquid chromatography-tandem mass spectrometry assays. In particular, Zn^{2+}-coordinated Cys139 and Cys142 mutations eliminated the H_2O_2 oxidation of PerR, and inductively coupled plasma mass spectrometry detected significantly decreased amounts of Zn^{2+} in H_2O_2-treated PerR, demonstrating that cysteine oxidation results in Zn^{2+} loss. An electrophoretic mobility shift assay (EMSA) determined that the DNA binding of Mn^{2+}-bound PerR protein (PerR:Zn,Mn) was abolished by H_2O_2 treatment but was restored by dithiothreitol reduction, verifying that H_2O_2 inactivates streptococcal PerR:Zn,Mn through cysteine oxidation, analogous to the findings for MntR. Quantitative PCR and EMSA demonstrated that *tpx*, *mntA*, *mntR*, and *dpr* belonged to the PerR regulons but that only *dpr* was directly regulated by PerR; *mntA* was also controlled by MntR. Deletion of *mntR* significantly reduced the low-H_2O_2-concentration-induced adaptation of *S. oligofermentans* to a higher H_2O_2 concentration, while the absence of PerR completely abolished the self-protection. Therefore, a low H_2O_2 concentration resulted in the cysteine-reversible oxidations of PerR and MntR to derepress their regulons, which function in cellular metal and redox homeostasis and which endow streptococci with the antioxidative capability. This work reveals a novel Cys redox-based H_2O_2 defense strategy employed by catalase-negative streptococci in Mn^{2+}-rich cellular environments.

IMPORTANCE The catalase-negative streptococci produce as well as tolerate high levels of H_2O_2. This work reports the molecular mechanisms of low-H_2O_2-concentration-induced adaptation to higher H_2O_2 stress in a *Streptococcus* species, in which the peroxide-responsive repressor PerR and its redox regulons play the major role. Distinct from the *Bacillus subtilis* PerR, which is inactivated by H_2O_2 through histidine oxidation by the Fe^{2+}-triggered Fenton reaction, the streptococcal PerR is inactivated by H_2O_2 oxidation of the structural Zn^{2+} binding cysteine residues and thus derepresses the expression of genes defending against oxidative stress. The reversible cysteine oxidation could provide flexibility for PerR regulation in streptococci, and the mechanism might be widely used by lactic acid bacteria, including

pathogenic streptococci, containing high levels of cellular manganese, in coping with oxidative stress. The adaptation mechanism could also be applied in oral hygiene by facilitating the fitness and adaptability of the oral commensal streptococci to suppress the pathogens.

KEYWORDS *Streptococcus*, cysteine oxidation, hydrogen peroxide, posttranslational regulation, redox signaling, transcriptional regulation

Reactive oxygen species (ROS), such as superoxide anions (O_2^-), hydrogen peroxide (H_2O_2), and hydroxyl radicals (HO·), damage almost all biological macromolecules (1–3). Therefore, organisms have evolved diverse mechanisms to cope with ROS (1–4). Facultatively anaerobic streptococci, such as the human opportunistic pathogen *Streptococcus pneumoniae* and the oral commensal bacterium *Streptococcus oligofermentans*, do not encode H_2O_2-scavenging catalase and thus accumulate endogenous H_2O_2 (5–8). Streptococci are also well-known for surviving in the presence of high concentrations of H_2O_2 (6, 9, 10). Previously, we determined that statically grown *S. oligofermentans* cultures have an approximately 200-fold higher survival rate than cells anaerobically cultured in 10 mM H_2O_2 (11). A similar observation has also been reported for *S. pneumoniae* (8). This suggests that the low levels of H_2O_2 that accumulate in statically cultured cells may assist streptococci with resisting the oxidant at higher concentrations. However, the biological basis of this low-H_2O_2-concentration-induced adaptation remains unknown.

Bacteria usually use cysteine-based redox reactions to sense H_2O_2 and activate the downstream peroxide detoxification pathways (12–14). *Escherichia coli* OxyR was the first identified archetype of thiol-based redox regulators in bacteria; it is activated by intramolecular thiol-disulfide formation resulting from H_2O_2 oxidation and thereby induces expression of the genes involved in defending against oxidative stress (15). Gram-positive bacteria, on the other hand, utilize the peroxide-responsive repressor PerR to sense H_2O_2 and derepress the H_2O_2 resistance genes (11, 16, 17). PerR, a member of the Fur family of metal-dependent regulators, possesses two metal-binding sites: a regulatory Fe^{2+} or Mn^{2+} binding site consisting of histidine and aspartate residues and a structural Zn^{2+} binding site comprising four cysteine residues (18, 19). The *Bacillus subtilis* PerR is inactivated by H_2O_2 via metal-catalyzed oxidation (MCO) (20). When binding Fe^{2+}, PerR is inactivated by Fenton chemistry-generated HO· from H_2O_2, which oxidizes the histidine residues. In contrast, the cysteine residues of the *B. subtilis* PerR that coordinate Zn^{2+} for structural maintenance are somehow inert to H_2O_2 (20). Therefore, PerR:Zn,Fe (Fe^{2+}-bound PerR) but not PerR:Zn,Mn responds to H_2O_2 (17, 19). Makthal et al. (21) also reported that H_2O_2 inactivates the recombinant *Streptococcus pyogenes* PerR:Zn,Fe, suggesting that Fe^{2+}-triggered Fenton chemistry could inactivate the streptococcal PerR as well. However, an *in vivo* study demonstrated that the *S. pyogenes* PerR:Zn,Mn also displays a weaker response to H_2O_2 (22). Previously, we found that the *S. oligofermentans* PerR is inactivated by H_2O_2 and derepresses the antioxidative non-heme iron-containing ferritin, *dpr*, and manganese importer *mntABC* genes (11). However, even if grown in Mn^{2+}-supplemented medium, H_2O_2 still induces the expression of *dpr*. This implies that the streptococcal PerR can be inactivated by mechanisms other than Fe^{2+}-triggered Fenton chemistry.

The redox-sensing transcriptional regulators usually respond to H_2O_2 challenge through cysteine oxidation (12, 13, 23). Recently, this thiol redox switch-based regulatory mechanism was found to be employed by other transcriptional regulators, such as AgrA in the control of the quorum sensing of *Staphylococcus aureus* (24) and MntR in the regulation of manganese uptake and the oxidative stress resistance of *S. oligofermentans* (25). Thiol redox proteomics is a powerful approach for the quantification of oxidative thiol modifications and the identification of physiologically important proteins in oxidative stress resistance (26–28). Using this approach, a number of novel redox-regulated proteins that contribute to the protection of *E. coli* from H_2O_2 stress (29) have been identified. Recently, proteome-wide quantification and characterization

TABLE 1 Prepulsing with a low H$_2$O$_2$ concentration increases the survival rates of various *S. oligofermentans* strains in the presence of a higher H$_2$O$_2$ concentration

	Survival rate (%)[a]			
Culture	Wild-type strain	Δ*pox* Δ*lox* mutant	Δ*mntR* mutant	Δ*perR* mutant
Static culture	30 ± 3.27*	0.02 ± 0.01*	ND	ND
Anaerobic culture				
Nonprepulse	0.21 ± 0.07	0.23 ± 0.06	7.94 ± 3.18	75 ± 11
Prepulse with 40 μM H$_2$O$_2$	77 ± 33	66 ± 12	62 ± 26	86 ± 14
Prepulse with 100 μM H$_2$O$_2$	46 ± 4	ND	ND	ND

[a]Strains were grown anaerobically in a 6-ml BHI culture, and then the survival percentages in 10 mM H$_2$O$_2$ were determined for all strains except for strains labeled with an asterisk, which were statically grown in a 40-ml culture and challenged with 20 mM H$_2$O$_2$. The survival percentage was calculated by dividing the number of CFU in the H$_2$O$_2$-treated culture by that in the untreated culture. The experiments were repeated three times with triplicate batch cultures each time. The results are averages ± SD from three independent experiments. ND, not determined.

of the oxidation-sensitive cysteine residues have determined complex and multilayered oxidative stress responses in pathogenic bacteria, such as *Pseudomonas aeruginosa*, *S. aureus*, and *S. pneumoniae* (8, 30). Therefore, cysteine-containing proteins not only serve as H$_2$O$_2$-damaged targets but also equip bacteria with the capability to resist H$_2$O$_2$ stress.

To elucidate the mechanisms underlying low-H$_2$O$_2$-concentration-induced resistance to high concentrations of H$_2$O$_2$ in streptococci, we employed physiological, biochemical, genetic, and redox proteomics approaches to investigate the H$_2$O$_2$-sensitive cysteine-containing proteins that may be involved in H$_2$O$_2$ adaptation. We determined that cellular H$_2$O$_2$ levels ranging from 40 to 100 μM protected *S. oligofermentans* from insult by higher H$_2$O$_2$ concentrations. Redox proteomics identified cysteine oxidation in the H$_2$O$_2$-responsive transcriptional regulators PerR and MntR, which regulate antioxidative stress in response to H$_2$O$_2$, as well as in the thioredoxin system proteins Tpx and Trx, which function in thiol-disulfide homeostasis. Importantly, 40 μM H$_2$O$_2$ oxidized the Zn^{2+}-coordinated cysteine residues and inactivated PerR, thus derepressing its regulons, which function in the thiol redox circuit and metal homeostasis. The high sensitivity of the cysteine residues to H$_2$O$_2$ enables PerR to sense low levels of H$_2$O$_2$ and thus protect the catalase-negative species *S. oligofermentans* from H$_2$O$_2$ challenge by maneuvering the H$_2$O$_2$ resistance systems. Moreover, the reversible cysteine oxidation resulting from a low H$_2$O$_2$ concentration can also endow the streptococcal PerR with flexibility in H$_2$O$_2$-responsive regulation.

RESULTS

Preexposure to a low H$_2$O$_2$ concentration enables *S. oligofermentans* to resist higher H$_2$O$_2$ concentrations. Previously, we found that aerobically cultured *S. oligofermentans* exhibits significantly higher resistance to H$_2$O$_2$ stress than anaerobic cultures (11), suggesting that the endogenous H$_2$O$_2$ that accumulates in the static culture may protect streptococci from damage in the presence of higher H$_2$O$_2$ concentrations. To validate this presumption, we deleted both the *pox* and *lox* genes, which encode pyruvate oxidase and lactate oxidase, respectively, the two major H$_2$O$_2$ producers in *S. oligofermentans* (5, 6). As expected, when exposed to 20 mM H$_2$O$_2$, only 0.02% survival was found for *pox lox* mutant cells; in comparison, 30% survival was found for wild-type cells (Table 1).

To verify if the loss of H$_2$O$_2$ resistance in the *pox lox* mutant was due to the lack of endogenous H$_2$O$_2$ but not the reduction of acetyl phosphate, which is produced by Pox and which contributes to *S. pneumoniae* H$_2$O$_2$ resistance (31), we determined whether a preexposure to a low concentration of H$_2$O$_2$ could increase the higher H$_2$O$_2$ resistance of the *pox lox* mutant. The wild-type and *pox lox* mutant strains were anaerobically grown until the optical density at 600 nm (OD$_{600}$) was ~0.5. One aliquot of the cultures, noted as the prepulse group, was pulsed for 20 min with 40 μM H$_2$O$_2$ prior to a 10-min

challenge with 10 mM H_2O_2. Another aliquot, the nonprepulse group, was directly treated with 10 mM H_2O_2. Samples not treated with 10 mM H_2O_2 were included as controls. Table 1 shows that prepulsing with 40 μM H_2O_2 greatly improved the survival of the *pox lox* mutant in the presence of 10 mM H_2O_2 to 66%, whereas that for the nonprepulsed group was 0.23%. Similarly, prepulsing with 40 μM H_2O_2 increased the survival rate of the wild-type strain to 77%, whereas that for the nonprepulsed group was 0.21%. Moreover, prepulsing with 100 μM H_2O_2 also elevated the survival rate of the wild-type strain to 46% in the presence of 10 mM H_2O_2 (Table 1). These results confirm that endogenous H_2O_2 at low concentrations plays an important role in the protection of *Streptococcus* from insult by a higher H_2O_2 concentration.

Estimation of endogenous H_2O_2 levels for self-protection and oxidative stress by HyPer fluorescent protein. Given that streptococci accumulate endogenous H_2O_2, we used the HyPer fluorescent protein to estimate intracellular H_2O_2 levels (32) and compared them with those excreted into the culture. The wild-type (WT) HyPer reporter strain of *S. oligofermentans*, WT-HyPer (33), was statically grown in 10, 20, 30, and 40 ml of brain heart infusion (BHI) broth in 100-ml flasks, which built an initial O_2 supply gradient. The growth profiles and the H_2O_2 amounts in the cultures were measured. Figure 1A shows that the best growth and the lowest H_2O_2 concentration (approximately 400 μM) were measured for the 40-ml culture. In contrast, the poorest growth and the highest H_2O_2 level (approximately 1,400 μM) were detected in the 10-ml culture, indicating that larger amounts of H_2O_2 are produced by *Streptococcus* with a rich supply of oxygen and thus suppress its growth.

Next, the mid-exponential-phase cells of the WT-HyPer strain from each volume of cultures were visualized under a confocal laser scanning microscope (Leica model TCS SP8), and the HyPer fluorescence intensities were measured as described in Materials and Methods. The Δpox-HyPer mutant, the *pox* deletion mutant carrying the HyPer gene (33), was included as a control from which H_2O_2 was absent. Figure 1B and C show that the HyPer fluorescence intensities were inversely proportional to the culture volumes but directly proportional to the H_2O_2 concentrations in the cultures, with a good linear regression ($R^2 = 0.8745$) (Fig. 1D). This indicates that the quantity of H_2O_2 in a culture indicates an equivalent amount within the cells.

Redox proteomics identifies cysteine-oxidized proteins by the low H_2O_2 concentration that induces self-protection from oxidative stress. To identify the proteins that are sensitive to a low H_2O_2 concentration and that might be involved in self-protection from oxidative stress, label-free redox proteomics analysis was performed to identify the cysteine-oxidized proteins in 40 μM H_2O_2-pulsed anaerobically grown *S. oligofermentans*. Proteins were extracted from H_2O_2-treated and -untreated cells, and cysteine thiol group oxidations were analyzed using a combination of differential alkylation and liquid chromatography (LC)-tandem mass spectrometry (MS/MS) (28, 34) (Fig. 2A). The representative MS/MS spectra shown in Fig. S1A and B in the supplemental material demonstrated the reliable identification of the cysteine-modified peptides.

LC-MS/MS identified 964 proteins in the samples not treated with H_2O_2 and 1,141 proteins in those pulsed with 40 μM H_2O_2; 923 were consistently detected in both samples. Among those, 93 cysteine-containing proteins were detected in H_2O_2-untreated cells and 132 were detected in 40 μM H_2O_2-treated cells (Data Set S1A to D). Proteins with reversible (S-S or SOH) or irreversible thiol oxidation (SO_2H or SO_3H) were identified by comparison with those in H_2O_2-untreated cells. The S-S oxidation ratio (in percent) in each sample was calculated by dividing the intensity of the disulfide-linked peptides by the sum of the peptides and considering a cutoff value of a $\geq$1.5-fold oxidation ratio in H_2O_2-treated cells over that in untreated cells to be significant (29). Proteins identified as SOH or SO_2H or SO_3H oxidations were those found only in H_2O_2-treated samples or with a $\geq$1.5-fold elevated peptide intensity compared to that for the control. In summary, 40 μM H_2O_2 treatment resulted in thiol group oxidation in 57 cysteine-containing proteins (Data Set S1E). Among these, 25 proteins containing 32 cysteine residues were oxidized into disulfide linkages (S-S), with a >50-fold increased
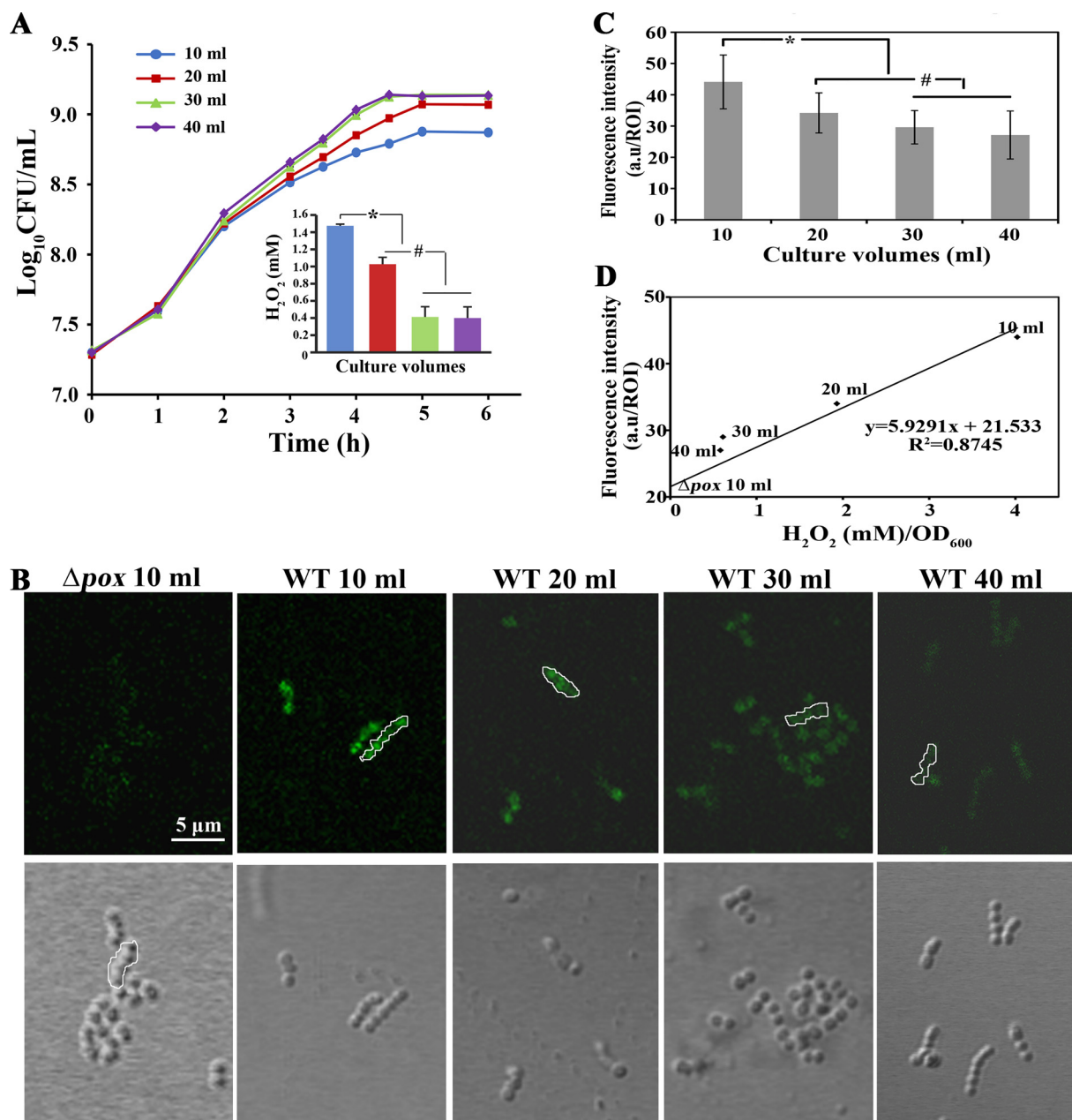
FIG 1 Correlation between growth suppression and the cellular H$_2$O$_2$ contents of *S. oligofermentans*. (A) An overnight culture of the HyPer reporter strain WT-HyPer was diluted 1:30 into 10, 20, 30, or 40 ml of BHI broth in 100-ml Erlenmeyer flasks and statically cultured at 37°C. Growth profiles were monitored by counting the numbers of CFU at the indicated time points. (Inset) H$_2$O$_2$ concentrations in the stationary-phase cultures were determined as described in Materials and Methods and are shown as bar diagrams using the color corresponding to the color of the growth curves for the same culture volumes. Experiments were conducted with three batches of culture and three replicates for each. Averages ± SD from three independent experiments are shown. * and #, the data are significantly different from those determined for 10-ml cultures and those determined for both the 10- and 20-ml cultures, respectively, as verified by one-way analysis of variance followed by Tukey's *post hoc* test ($P < 0.05$). (B) One milliliter of mid-exponential-phase WT-HyPer cells was collected from the cultures for which the results are shown in panel A, washed twice with PBS, and resuspended in 100 μl PBS. After a 30-min air exposure in the dark, HyPer fluorescence was examined using a confocal laser scanning microscope system (Leica model TCS SP8). The Δ*pox*-HyPer cells grown in 10 ml of culture were included as an endogenous H$_2$O$_2$-negative control. Representative fluorescent and corresponding differential interference contrast (DIC) images from three independent experiments are shown. (C) The HyPer fluorescence intensities of the cells shown in panel B were measured using Leica Application Suite (LAS) AF software. At least five images were captured per sample, and 25 regions of interest (ROI; outlines framed in panel B), each containing 5 cells, were measured for calculation of the average fluorescence intensity of each sample. For images with fluorescence that was too weak, the ROI in the corresponding DIC images was framed, and the fluorescence in the corresponding ROI of the fluorescence image was measured. Average fluorescence intensities were calculated and are expressed in arbitrary units (a.u.) per ROI ± standard deviation. *and #, data are significantly different from those obtained from 10-ml cultures and those determined from both 10- and 20-ml cultures, respectively ($P < 0.05$, one-way analysis of variance followed by Tukey's *post hoc* test). (D) A linear regression curve of the HyPer fluorescence intensities in Δ*pox*-HyPer and WT-HyPer cells plotted against the extracellular H$_2$O$_2$ concentrations in the corresponding culture volumes.
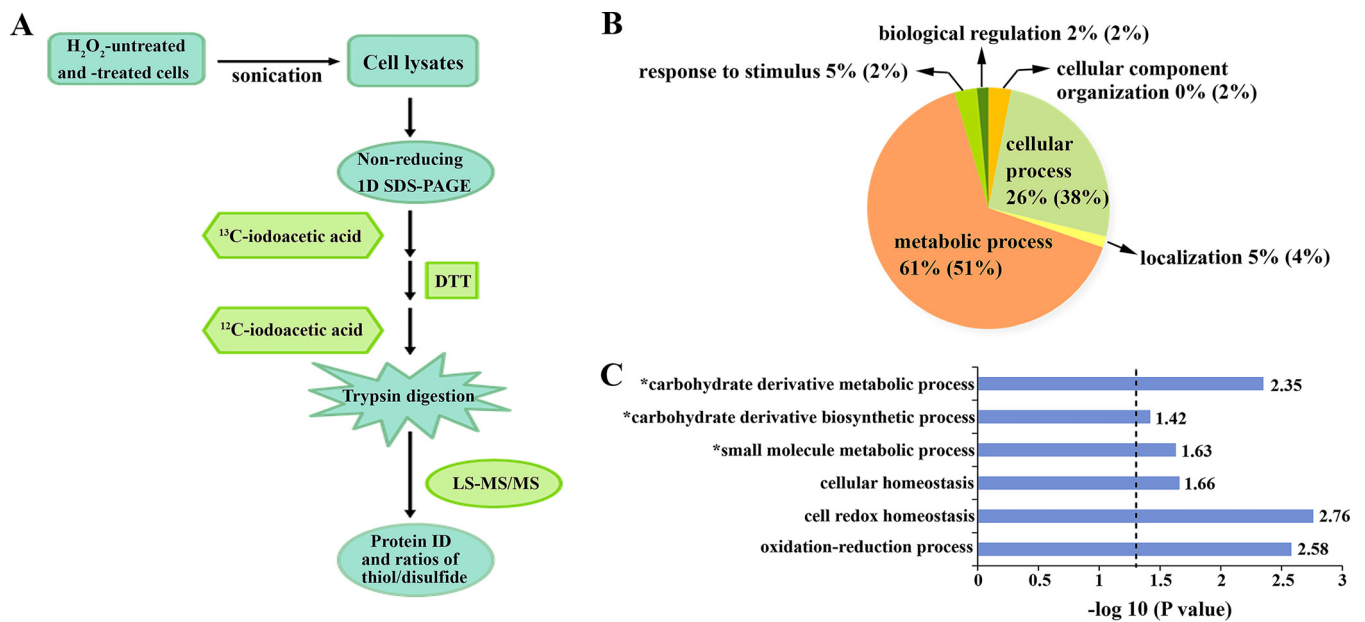
FIG 2 Redox proteomic identification of proteins whose cysteines were oxidized by endogenous or exogenous H_2O_2 at levels protecting *S. oligofermentans* from oxidative stress. (A) Flowchart of redox proteomic analysis, performed using differential alkylation and LC-MS/MS. The free and disulfide-oxidized thiol groups were modified by [^{13}C]- and [^{12}C]iodoacetic acid, respectively. Detailed experimental procedures are described in Materials and Methods. 1D, one dimensional; ID, identifier. (B) Functional classification of the proteins with cysteine residues reversibly or irreversibly oxidized in the wild-type strain statically grown in a 40-ml culture and the 40 μM H_2O_2-pulsed anaerobically grown wild-type strain (percentages in parentheses), based on Gene Ontology (GO) analysis. (C) Overrepresented biological processes associated with cysteine-oxidized proteins were examined using a statistical overrepresentation test on the Gene Ontology Consortium website. The binomial test was used for statistical significance analysis using a P value of <0.05 as a cutoff, which is indicated by a dashed line. Asterisks indicate the biological processes enriched in both 40 μM H_2O_2-pulsed cells and cells grown in the 40-ml culture. The remaining items were enriched only in cells grown in the 40-ml culture.

disulfide ratio in 21 proteins; 3 proteins were reversibly oxidized as SOH; and the remaining 29 proteins were irreversibly oxidized as SO_2H or SO_3H. Thus, these 57 proteins are assumed to be involved in self-protection from H_2O_2 challenge.

As *S. oligofermentans* cells statically grown in the 40-ml culture survived the 20 mM H_2O_2 challenge (Table 1), we identified the cysteine-oxidized proteins in this volume of culture. A total of 1,093 proteins were identified by LC-MS/MS analysis, including 108 cysteine-containing proteins (Data Set S2A and B). Calculations indicated that 35 proteins were oxidized, with 26 cysteine residues in 23 proteins being reversibly oxidized into disulfide linkages (S-S) and the remaining 12 proteins being irreversibly oxidized as SO_2H or SO_3H (Data Set S2E). However, in cells cultured in 10-ml cultures that accumulated larger amounts of H_2O_2, 66 of the 164 cysteine-containing proteins were oxidized, with 33 being oxidized as S-S and 33 being oxidized as SO_2H or SO_3H (Data Set S2C to E). Thirty-one proteins that were specifically oxidized in 10- ml cultures belonged to organic acid and organic nitrogen metabolic processes (Data Set S2F), accounting for the growth retardation of *S. oligofermentans* under oxidative stress.

To link the biological functions of the H_2O_2-sensitive proteins, Gene Ontology (GO) analysis was performed by use of the PANTHER bioinformatics platform (http://www.pantherdb.org/) (35). Figure 2B shows that the proteins oxidized by endogenous H_2O_2 (in 40-ml aerobic cultures) and exogenously provided H_2O_2 (for 40 μM H_2O_2-pulsed anaerobic cells) were categorized into similar biological processes, with approximately 61% and 51% of the proteins, respectively, being involved in metabolic processes and 26% and 38% of the proteins, respectively, being involved in cellular processes. Remarkably, almost all the proteins in the glycolysis and nucleotide salvage pathways were oxidized to form disulfide linkages (Table 2; Fig. 2C; Data Sets S1F and S2F). As expected, the antioxidative thiol-reducing proteins thiol peroxidase (Tpx) and thioredoxin (Trx) were 36.5% to 100% oxidized. It is worth noting that the metalloregulator MntR was markedly oxidized at the thiol group of cysteines (Table 2; Data Sets S1E and

TABLE 2 Redox proteomics identified the cysteine residues and proteins of *S. oligofermentans* oxidized by both an exogenous 40 μM H₂O₂ pulse and endogenous H₂O₂ produced in 40-ml static cultures

No.	Accession no. in KEGG database	Protein description	Peptide sequence	Modified cysteine	Thiol/disulfide oxidized ratio (%)[a]		
					40-ml culture	Nonpulsed culture	40 μM H₂O₂-pulsed culture
1	I872_01020	Metal-dependent transcriptional regulator	CIYEIGTR	C11	100	0	100*
2	I872_09155	Glyceraldehyde-3-phosphate dehydrogenase	TIVFNTNHDVLDGTETVISGASCTTNCLAPMAK	C151, C155	C151, 24.7; C155, 100	0	C151, SO₃H; C155, 100*
3	I872_08015	Fructose-bisphosphate aldolase	VNVNTECQIAFANATR	C235	100	0.5 $\pm$ 0.5	100*
4	I872_06890	Pyruvate kinase	AICEETGNGHVQLFAK	C235	100	0	57.4 $\pm$ 24.9*
5	I872_00255	Aldehyde-alcohol dehydrogenase	IAEPVGVVCGITPTTNPTSTAIFK	C120	100	0	100*
6	I872_10355	6-Phospho-beta-glucosidase	NVETCLAQPVLLR	C318	100	0	100*
7	I872_00060	Hypoxanthine phosphoribosyltransferase	NLCNLFK	C112	100	0	100*
8	I872_01620	Protein translocase subunit SecA	ELGGLCVIGTER	C507	100	10 $\pm$ 10	98 $\pm$ 2*
9	I872_09640	Probable thiol peroxidase	VLSIVPSIDTGVCSTQTR	C58	100	0	36.5 $\pm$ 3.5*
10	I872_03205	Thioredoxin family protein	FWASWCGPCK[b]	C82	10	80	100
11	I872_00600	50S ribosomal protein L36	VMVICPANPK	C27	100	24 $\pm$ 6	100*

[a]The thiol/disulfide oxidized ratio was calculated by dividing the intensity of oxidized disulfide-linked peptide by the sum of the intensities of the oxidized and reduced peptides in the corresponding sample. *, a cutoff of a $\geq$1.5-fold oxidation ratio in H₂O₂-treated cells over that in untreated cells was considered significant. Experiments were repeated twice, and the results are the averages $\pm$ SD from two independent experiments.
[b]This peptide fragment was detected in only one independent experiment.

S2E). In a preliminary redox proteomic experiment, 40 μM H₂O₂ treatment also resulted in the oxidations of Cys139 and Cys142 of the peroxide-responsive repressor PerR (Fig. S1C). The consistently identified redox-sensitive proteins in the 40-ml cultures and 40 μM H₂O₂-pulsed cells (Table 2) either might be involved in self-protection or might simply be hypersensitive to oxidative damage.

Redox Western blotting validates the oxidation of cysteine-containing proteins by a low H₂O₂ concentration, notably, the cysteine oxidation of PerR. To verify the redox proteomics-identified cysteine residues sensitive to low H₂O₂ concentrations, Tpx and Trx, the well-known antioxidative proteins, were chosen to examine cysteine oxidation by 40 μM H₂O₂ in Tpx-6×His and Trx-6×His strains, which carried a 6×His tag fusion at the C terminus of the Tpx and Trx proteins, respectively. Redox Western blotting was performed as described in Materials and Methods. As shown in Fig. 3A, in comparison with the migration of Tpx from H₂O₂-untreated Tpx-6×His cells (lane 1), a similar faster-migrating band was also detected for both Tpx from H₂O₂-treated cells (lane 2) and the recombinant Tpx-6×His protein (lane 3), which could be partially oxidized during purification, while upon dithiothreitol (DTT) reduction, the faster-migrating Tpx band from H₂O₂-treated cells and the Tpx-6×His protein disappeared (lanes 4, 5, and 6). This indicates that H₂O₂ oxidation results in an intramolecular disulfide linkage in Tpx. Consistently, LC-MS/MS identified the thiol oxidation of Cys58 (Fig. 3C; Fig. S1E and F), and H₂O₂ treatment caused approximately 36% of the Tpx protein to be oxidized (Fig. 3C; Table 2; Data Set S1E). Although redox proteomics identified Trx Cys82 to be complete oxidized (Fig. 3D; Fig. S1I), redox Western blotting did not detect a differential migration of the Trx protein upon H₂O₂ oxidation or DTT reduction (Fig. 3B, lanes 1 and 2 versus lanes 5 and 6), while addition of 4-acetamido-4′-maleimidylstilbene-2,2′-disulfonic acid (AMS), a free thiol-reactive reagent, generated different upshifted Trx bands by higher upshifting in DTT-reduced cells than in H₂O₂-treated cells (Fig. 3B, lanes 4 and 8 versus lanes 3 and 7). By reference to an apparent molecular weight increase of 500 Da per AMS molecule (36) and the migration of three AMS-bound recombinant Trx-6×His proteins (Fig. 3B, lane 10), the differential protein migration in H₂O₂-treated and DTT-reduced cells suggests that a reversible thiol group oxidation (–SOH) in one cysteine of Trx is formed by H₂O₂
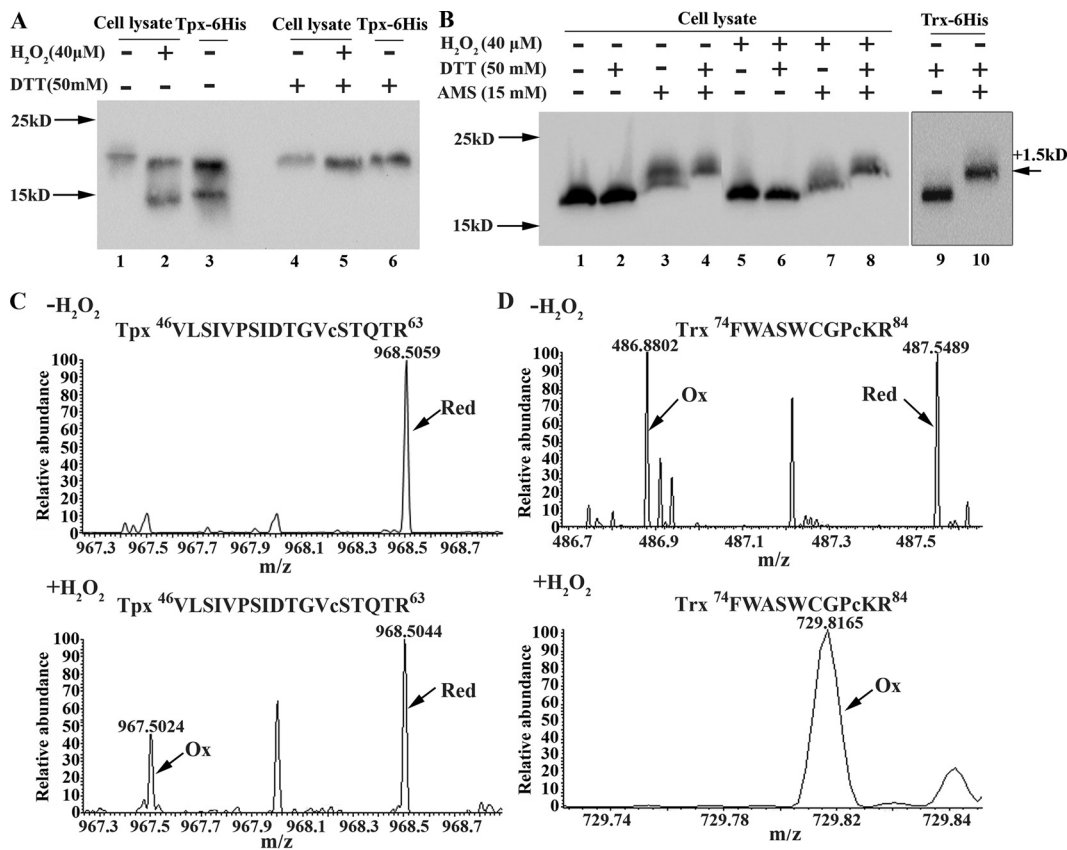
FIG 3 Verification of the cysteine oxidation of thiol peroxidase (Tpx) and thioredoxin (Trx) in 40 µM H$_2$O$_2$-treated anaerobic cultures. (A) A 6×His tag was fused to the C terminus of the *tpx* gene (KEGG accession number I872_09640) to construct the *S. oligofermentans* Tpx-6×His strain. Mid-exponential-phase anaerobically grown Tpx-6×His cells were treated with or without 40 µM H$_2$O$_2$ for 20 min, collected inside an anaerobic glovebox, and then lysed in RIPA buffer containing the free thiol protectant NEM. The cell lysate of each sample was divided into two aliquots; one was left untreated (lanes 1 and 2), and the other was reduced with 50 mM DTT for 1 h (lanes 4 and 5). Redox Western blotting was carried out using an 18% SDS-PAGE gel to detect the Tpx-6×His protein using an anti-His tag antibody. Recombinant Tpx-6×His protein, which was partially oxidized and which formed an intramolecular disulfide linkage during purification, was treated with or without 50 mM DTT (lanes 3 and 6) and used as a reduced and an oxidized molecular control, respectively. (B) Using the same approach described in the legend to panel A, a disulfide linkage upon 40 µM H$_2$O$_2$ oxidation was identified for thioredoxin (KEGG accession number I872_03205) in the Trx-6×His strain (lanes 1 and 2 versus lanes 5 and 6). In addition, 15 mM 4-acetamido-4'-maleimidylstilbene-2,2'-disulfonic acid (AMS), the free thiol-chelating reagent, was used to detect the nondisulfide oxidation of the thiol groups (lanes 3 and 4 and lanes 7 and 8). Cell lysates from the H$_2$O$_2$-untreated strain (lanes 3 and 4) and the H$_2$O$_2$-treated Trx-6×His strain (lanes 7 and 8) were reduced with or without 50 mM DTT. The recombinant Trx-6×His protein was first reduced by 50 mM DTT, and then one aliquot was alkylated with AMS and another was left untreated; these were used as reduced and thiol AMS-bound Trx-6×His protein controls, respectively (lanes 9 and 10). Molecular weight markers are shown at the left, and the increased molecular weight of the protein due to bound AMS molecules (500 Da each) is shown at the right. (C and D) Redox proteomics identified the reduced (Red) and oxidized (Ox) peptide fragments of Tpx VLSIVPSIDTGVC^{58}STQTR (C) and Trx FWASWCGPC^{82}KR (D) in H$_2$O$_2$-untreated (top) and H$_2$O$_2$-treated *S. oligofermentans* cells (bottom). The relative abundances of the oxidized and reduced peptide fragments are shown.

treatment. Therefore, redox Western blotting confirmed the oxidation of cysteine residues in cells treated with a low concentration of H$_2$O$_2$.

Previously, we demonstrated that the peroxide-responsive repressor PerR and the metalloregulator MntR are involved in the H$_2$O$_2$ resistance of *S. oligofermentans* (11, 25). Interestingly, redox proteomics detected the cysteine oxidation of the two proteins in 40 µM H$_2$O$_2$-treated cells. Recently, we have validated the increased amount of disulfide-linked MntR oligomer in 40 µM H$_2$O$_2$-pulsed cells (25). Here, we examined H$_2$O$_2$-caused cysteine oxidation in PerR. A PerR-6×His strain, which carries a 6×His tag fusion at the C terminus of PerR, was treated with or without 40 µM H$_2$O$_2$ and then lysed in the presence of the free thiol protectant *N*-ethylmaleimide (NEM) and 10 mM EDTA, which chelates Fe^{2+} and so avoids Fenton chemistry-mediated PerR oxidation, as demonstrated in *B. subtilis* PerR (20). Redox Western blotting detected two bands in the

H_2O_2-untreated PerR-6×His culture, whereas the upper band appeared mainly in the H_2O_2-treated culture and the lower one appeared exclusively in DTT-treated cell lysates (Fig. 4A, lanes 1 to 4, and Fig. 4B). This is reminiscent of the findings for *B. subtilis* PerR, which migrated more slowly when the structure maintaining Zn^{2+} was lost due to the oxidation of cysteine residues (20). Therefore, AMS was employed to examine the cysteine redox status of PerR from H_2O_2-treated PerR-6×His cells. Figure 4A shows that AMS addition increased the apparent molecular weight of PerR from DTT-reduced cell lysates (upshifted at approximately 0.5 cm, lane 6 versus lane 4) compared to that of PerR from the non-DTT-reduced ones (upshifted at approximately 0.3 cm, lane 5 versus lane 3). This indicates that some but not all of the four Cys residues of the streptococcal PerR are oxidized by pulsing with a low H_2O_2 concentration.

Redox Western blotting indicated that PerR was also oxidized in statically grown cells (Fig. S2A). To further verify the endogenous cysteine oxidation resulting from H_2O_2, 6×His-tagged PerR protein immunoprecipitated from statically grown cells was subjected to differential alkylation and LC-MS/MS analysis (Fig. S2B). Figure 4D displays the representative MS/MS spectra of the peptide fragments carrying four cysteine residues. By counting the peptide fragments carrying oxidative and reductive cysteine residues, we calculated the oxidation ratios of the four cysteine residues to be 76% (Cys100), 50% (Cys103), 83% (Cys139), and 82% (Cys142) (Table S1), whereas His40 and His95, whose oxidations inactivate *B. subtilis* PerR (20), were oxidized approximately 28% and 53%, respectively, in *S. oligofermentans* PerR (Table S1). Collectively, both MS/MS identification and redox Western blotting determined that the Zn^{2+}-coordinated cysteine residues of *S. oligofermentans* PerR are hypersensitive to H_2O_2 oxidation.

H_2O_2 oxidation of the cysteine residues abolishes PerR binding to DNA due to Zn^{2+} loss. To further determine whether H_2O_2 oxidation occurs at the cysteine residues of the streptococcal PerR *in vivo*, Cys139 and Cys142 were replaced by serine on the shuttle plasmid pDL278-*perR*-6×His. Wild-type *perR* and cysteine-mutated *perR* were each ectopically expressed in a *perR* deletion strain, and the resultant complementary strains were treated with or without 40 µM H_2O_2. Redox Western blotting showed that, different from the findings for wild-type PerR, cysteine-mutated PerR retained the same migration in all samples regardless of 40 µM H_2O_2 oxidation or DTT reduction (Fig. 4B). This result demonstrates that H_2O_2 oxidizes Cys139 and Cys142 of the streptococcal PerR.

It is worth noting that even if cells were collected inside an anaerobic glove box and lysed in the presence of NEM, EDTA, and catalase, part of the PerR protein was still oxidized (Fig. 4A, lane 1), suggesting the PerR cysteine residues are hypersensitive to oxidants. This was further confirmed by redox Western blotting, which detected oxidized PerR protein from the cells pulsed by 40 µM H_2O_2 for only 1 min (Fig. 4C). Noticeably, invariable lower Western blotting signals were detected for PerR from H_2O_2-treated cells than for PerR from DTT-reduced cells, and this was determined to be because DTT increased the anti-His tag antibody signal (Fig. S3).

By reference to the *B. subtilis* PerR and other Cys_4Zn proteins, such as Hsp33 and RsrA (37, 38), oxidation of Zn^{2+}-coordinated cysteine residues would cause Zn^{2+} loss and, therefore, slower protein migration because of the conformational changes. We subsequently verified whether H_2O_2 oxidation causes Zn^{2+} loss from PerR. Overexpressed glutathione *S*-transferase (GST)-tagged PerR protein (GST-PerR) was treated or not treated with 5 mM H_2O_2 and subsequently reduced or not reduced with 50 mM DTT. Nonreducing SDS-PAGE analysis did reveal a slower-migrating band for the 5 mM H_2O_2-treated protein than for the DTT-treated protein (Fig. 5A). Inductively coupled plasma mass spectrometry (ICP-MS) also determined 0.09 mol of Zn^{2+} per mol of H_2O_2-treated PerR and 0.79 mol of Zn^{2+} per mol of DTT-reduced PerR (Fig. 5B), confirming that H_2O_2 oxidation causes Zn^{2+} loss from PerR.

Next, we determined whether Zn^{2+} loss affects DNA binding by PerR. Fifty nanomoles of PerR:Zn,Mn was used for a electrophoretic mobility shift assay (EMSA), based on a calculated K_d (dissociation constant) value of approximate 50 nM for binding (Fig. 5C). Figure 5D shows that 50 µM H_2O_2 treatment for 30 min diminished PerR's binding to the
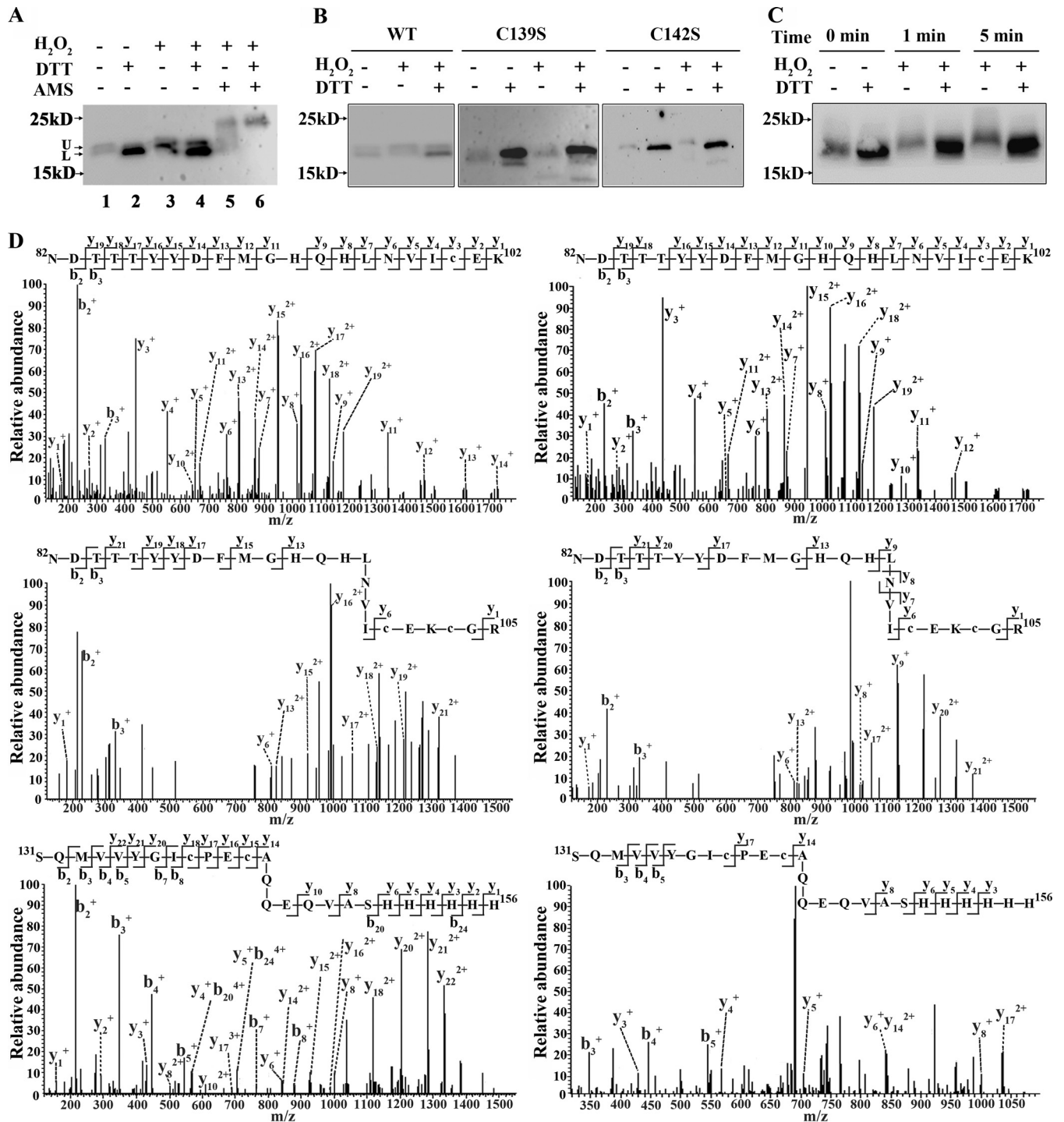
FIG 4 Assay of PerR cysteine oxidation in 40 μM H_2O_2-treated cells. (A) A 6×His tag was fused to the C terminus of *perR* (KEGG accession number I872_05555) to construct the *S. oligofermentans* PerR-6×His strain. Using the same approach described in the legends to Fig. 3A and B, redox Western blotting detected cysteine oxidation in the 6×His-tagged PerR protein using the anti-His tag antibody. U and L at the gel left indicate upper and lower protein bands, respectively. (B) A serine substitution of either Cys139 or Cys142 was constructed on a shuttle plasmid (pDL278-*perR*-6×His), and the plasmid was transformed into the *perR* deletion strain to construct the *perR*::pDL278-*perR*C139S-6×His (C139S) and *perR*::pDL278-*perR*C142S-6×His (C142S) strains. The *perR* deletion mutant harboring pDL278-*perR*-6×His (WT) was included as a control. The three strains were anaerobically cultured and then treated with 40 μM H_2O_2. Redox Western blotting, as described in the legend to Fig. 3A, was carried out to detect the oxidation of the PerR mutants. (C) The PerR-6×His strain was anaerobically cultured, and cells were treated with 40 μM H_2O_2 for 1 min and 5 min. Using the methods described in the legend to Fig. 3A, the cysteine oxidation of PerR was detected by redox Western blotting. (D) The 6×His-tagged PerR protein was immunoprecipitated from the statically grown PerR-6×His strain as described in Materials and Methods and then resolved on an 18% nonreducing SDS-PAGE gel. The protein band was then subjected to differential alkylation and LC-MS/MS analysis. (Top) Representative MS/MS spectra of the triply charged peptide ions at *m/z* 863.7217 and 862.7243, corresponding to reduced (left) and oxidized (right) NDTTTYYDFMGHQHLNVIC^{100}EK peptide fragments, respectively. (Middle) Representative MS/MS spectra of triply charged peptide ions at *m/z* 989.1003 and 992.4445, corresponding to both Cys100 and Cys103 reduced (left) and oxidized (right) NDTTTYYDFMGHQHLNVIC^{100}EKC^{103}GR peptide fragments, respectively.

(Continued on next page)

dpr promoter (lane 5) and that 200 µM H$_2$O$_2$ treatment completely abolished the binding (lane 6); meanwhile, 10 mM DTT reduction recovered the binding (lane 9 versus lane 10), indicating that PerR is reversibly inactivated by H$_2$O$_2$ oxidation at cysteine residues. Moreover, 5 min of treatment with 200 µM H$_2$O$_2$ inactivated approximately 59% of the PerR protein (Fig. 5E and F). It is worth noting that the EMSA buffer was treated with Chelex 100 to chelate metal ions that might trigger the Fenton reaction. Noticeably, LC-MS/MS did not detect increased histidine residue oxidation in the H$_2$O$_2$-treated PerR:Zn,Mn protein (Table S2), while histidine oxidations that occurred before H$_2$O$_2$ treatment might have been generated during the *in vitro* purification. In conclusion, H$_2$O$_2$ oxidizes cysteine residues but not histidine residues and inactivates PerR.

PerR and MntR regulate the cellular redox system and metal homeostasis. Trx and Tpx are involved in cellular redox homeostasis and belong to the *S. aureus* and *Clostridium acetobutylicum* PerR regulons (39, 40). Additionally, Dpr, a non-heme iron-containing ferritin, and MntABC, a manganese ABC transporter, are known to play important roles in maintaining cellular metal homeostasis and are under the control of *S. oligofermentans* PerR and MntR (11, 25). To determine whether the four genes mentioned above plus *mntR* belong to the PerR or MntR regulons, we performed quantitative PCR (qPCR) to quantify the expression of these genes in 40 µM H$_2$O$_2$-pulsed and nonpulsed anaerobically grown wild-type strain and *perR* deletion, *mntR* deletion, and *perR mntR* double deletion mutants. In comparison with the 40 µM H$_2$O$_2$-induced 3- to 5.8-fold higher levels of expression of *tpx*, *dpr*, *mntA*, and *mntR* in the wild-type strain, deletion of *mntR* abolished the H$_2$O$_2$ induction of *mntA*; however, the H$_2$O$_2$ induction of the four genes almost disappeared in the mutants either with a deletion of *perR* or with a deletion of both *perR* and *mntR* (Table 3). These demonstrate that the H$_2$O$_2$-induced expressions of *tpx*, *dpr*, *mntA*, and *mntR* are under the control of PerR, while *mntA* is also controlled by *mntR* in response to H$_2$O$_2$.

Notably, even in the absence of H$_2$O$_2$, 2.5- to 4.0-fold higher levels of expression of *tpx*, *dpr*, and *mntA* were detected in the ΔperR and ΔperR ΔmntR mutants than in the wild-type strain, suggesting that PerR may directly regulate the *tpx*, *dpr*, and *mntA* genes. However, the conserved PerR binding sequence (TTAATTAGAAGCATTATAAT TAA) was found only in the *dpr* promoter region; consistently, EMSA indicated PerR binding to the *dpr* promoter (Fig. 5C) but not to the promoters of *mntABC*, *tpx*, and *mntR* (Fig. S4). Our previous work found that MntR bound to the *mntABC* promoter (25), indicating the direct regulation of *mntA* by MntR. Thus, PerR directly regulates *dpr* but indirectly regulates *mntA*, *tpx*, and *mntR* via unknown mechanisms. Of note, similar expression levels of the PerR-regulated genes were detected in cells pulsed only with 40 µM H$_2$O$_2$ and cells that were pulsed and then further challenged by 10 mM H$_2$O$_2$ (Table 3), indicating that these genes are under the control of PerR, which is already inactivated by as little as 40 µM H$_2$O$_2$.

PerR, MntR, and the regulated cellular redox and metal homeostatic proteins are involved in the self-protection of *S. oligofermentans* from H$_2$O$_2$ stress. Given that both PerR and MntR contribute to the high H$_2$O$_2$ resistance of *S. oligofermentans* (11, 25), to determine their roles in self-protection against H$_2$O$_2$ stress, the ΔperR and ΔmntR mutants were prepulsed with or without 40 µM H$_2$O$_2$, and then their survival with 10 mM H$_2$O$_2$ challenge was determined as described above. Table 1 shows that the *mntR* deletion dramatically reduced the 40 µM H$_2$O$_2$-induced protection from high H$_2$O$_2$ challenge to 8-fold, compared to the 367-fold protection in the wild-type strain, while *perR* deletion almost completely abolished the low-H$_2$O$_2$-concentration-induced adaptation (Table 1). Together, the two redox regulators MntR and, in particular, PerR play important roles in the low-H$_2$O$_2$-concentration-induced self-protection of *S. oligo-fermentans* from a higher-concentration H$_2$O$_2$ stress, most likely by H$_2$O$_2$ inactivating

FIG 4 Legend (Continued)
(Bottom) The MS/MS spectra represent triple- and quintuple-charged peptide ions at *m/z* 1038.1281 and 622.0834, respectively, corresponding to both Cys139 and Cys142 reduced (left) and oxidized (right) SQMVVYGIC[139]PEC[142]AQQEQVASHHHHHH peptide fragments. The reduced and oxidized cysteine residues were ^{13}C carboxymethylated and ^{12}C carbamidomethylated, respectively.
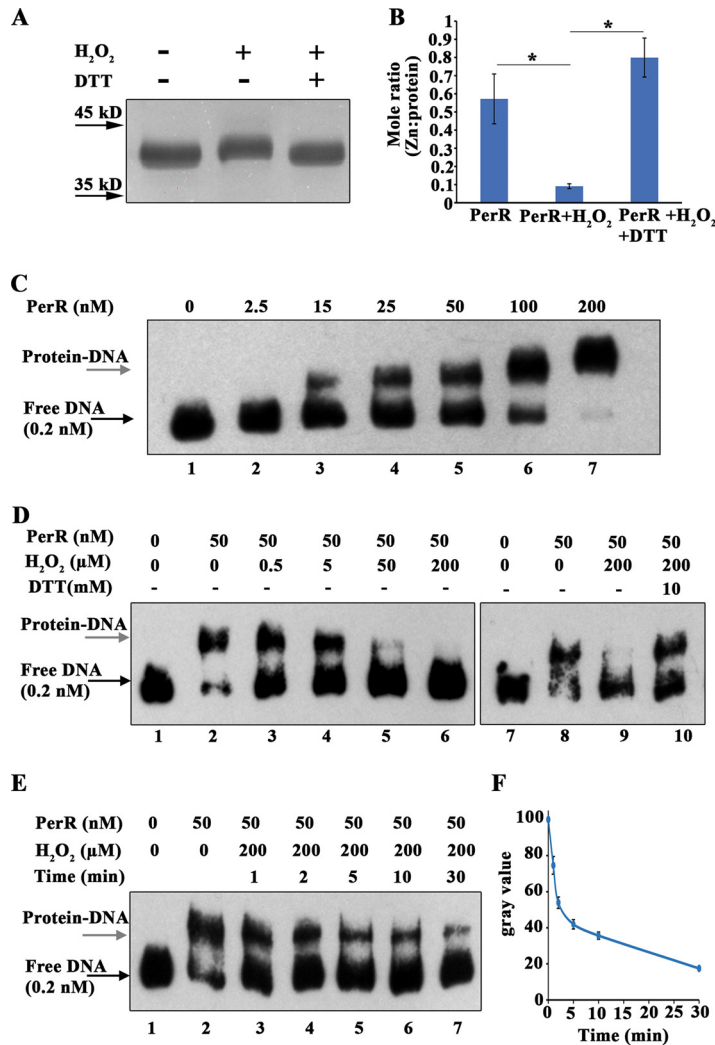
FIG 5 Determination of zinc ion loss and inactivation of the PerR protein caused by H_2O_2 oxidation. (A and B) The recombinant PerR-GST protein was purified in PBS buffer containing 10 mM EDTA and 3 mM GSH, as described in Materials and Methods. Purified PerR-GST was divided into three aliquots: one was not treated, and the remaining two were treated for 30 min with 5 mM H_2O_2, with one of these two aliquots subsequently being subjected to 1 h of reduction with 50 mM DTT. Aliquots of the three protein samples were resolved on nonreducing 18% SDS-PAGE gels, and the remaining samples were ultrafiltered and, finally, resuspended in 650 μl PBS buffer. The protein concentrations of PerR-GST were determined using a BCA protein assay kit, and the zinc concentration in the protein was measured using ICP-MS. The molar ratios of zinc ion to the PerR-GST monomer were calculated. The averages ± SD from three independent experiments are shown. *, a result significantly different from that for H_2O_2-treated PerR-GST protein, as verified by one-way analysis of variance followed by Tukey's *post hoc* test ($P < 0.05$). (C) The PerR-GST protein was digested with 100 U thrombin to remove the GST tag and then eluted into a buffer containing 10 mM EDTA and 1 mM DTT. Next, 1 μM PerR protein was preincubated with 1 mM $MnCl_2$, and then gradient concentrations of the recombinant PerR:Zn,Mn protein (0 to 200 nM) were tested for binding to the 5′-biotin-labeled *dpr* promoter fragment, as described in Materials and Methods. (D) One micromole of PerR protein was incubated with 1 mM $MnCl_2$ and then treated with increasing concentrations of H_2O_2 at 30°C for 30 min. After incubation, 150-U/ml catalase was added to decompose the residual H_2O_2, and 50 nM PerR protein was used for EMSA to test the affinity of binding to the *dpr* promoter (lanes 3 to 6). To observe whether the H_2O_2 oxidation-diminished PerR binding could be restored, 10 mM DTT was added to the 200 μM H_2O_2-treated PerR and the mixture was incubated at 37°C for 1 h (lane 10). E. One micromole of the PerR protein was preincubated with 1 mM $MnCl_2$ and then treated with 200 μM H_2O_2 at 30°C for different times (lanes 3 to 7). Fifty nM PerR protein was used in the EMSA. Black and gray arrows point to the free DNA probe and protein-DNA complex, respectively. (F) Band densities of the protein-DNA complex in lanes 2 to 7 of panel E were evaluated using ImageJ software, with the density in lane 2 being set as 100%. The density percentages in lanes 3 to 7 were calculated by dividing the band density of the respective lane by that of lane 2. All the experiments were repeated three times, and the averages ± SD from three independent experiments are shown.

TABLE 3 Identification of the PerR regulon by qPCR quantification of the gene transcript copies in anaerobically grown wild-type and *perR* and *mntR* single and double deletion strains with and without 40 μM H$_2$O$_2$ treatment

	Transcript copy no./100 16S rRNA copies[b]								
	Wild-type strain			$\Delta perR$ mutant		$\Delta mntR$ mutant		$\Delta perR$ $\Delta mntR$ mutant	
Gene[a]	Without H$_2$O$_2$	With H$_2$O$_2$	With H$_2$O$_2$ + high[c]	Without H$_2$O$_2$	With H$_2$O$_2$	Without H$_2$O$_2$	With H$_2$O$_2$	Without H$_2$O$_2$	With H$_2$O$_2$
mntR	0.76 ± 0.05	2.35 ± 0.21*	2.16 ± 0.31*	0.77 ± 0.12	0.83 ± 0.02	ND	ND	ND	ND
mntA	5.52 ± 1.50	18.04 ± 3.75*	20.75 ± 4.74*	13.81 ± 0.93*	21.70 ± 3.94*	18.70 ± 1.59*	19.70 ± 0.36*	18.94 ± 2.02*	22.47 ± 3.53*
dpr	6.26 ± 2.18	34.92 ± 6.40*	29.54 ± 4.74*	21.40 ± 2.80*	27.91 ± 0.16*	7.89 ± 0.76	23.62 ± 2.47*#	25.01 ± 0.26*	30.77 ± 6.82*
tpx	0.56 ± 0.11	3.22 ± 0.17*	3.10 ± 0.23*	1.30 ± 0.19*	1.45 ± 0.24*	0.66 ± 0.02	1.78 ± 0.10*#	1.60 ± 0.08*	1.71 ± 0.39*
trx	0.73 ± 0.17	1.35 ± 0.35	0.75 ± 0.34	0.96 ± 0.12	1.36 ± 0.18	0.82 ± 0.19	0.79 ± 0.09	0.62 ± 0.02	0.80 ± 0.16

[a] *mntR*, Mn-dependent transcriptional regulator (KEGG accession number I872_01020); *mntA*, manganese transport system substrate-binding protein (KEGG accession number I872_09645); *dpr*, non-heme iron-containing ferritin (KEGG accession number I872_07415); *tpx*, thiol peroxidase (KEGG accession number I872_09640); *trx*, thioredoxin (KEGG accession number I872_03205).

[b] The experiments were repeated three times with triplicate batch cultures each time. The results are the averages ± SD from three independent experiments. The data were significantly different from those obtained for the wild-type strain without 40 μM H$_2$O$_2$ treatment (*) and from those obtained with the same strain not treated with H$_2$O$_2$ (#), as verified by one-way analysis of variance followed by Tukey's *post hoc* test ($P < 0.05$). ND, not determined.

[c] qPCR was implemented with the wild-type strain prepulsed with 40 μM H$_2$O$_2$ and then further challenged by 10 mM H$_2$O$_2$.

the two transcriptional repressors and thereby derepressing the antioxidative systems. Notably, a 9.4-fold elevated survival rate in the presence of a higher concentration of H$_2$O$_2$ was observed for the $\Delta perR$ mutant than for the $\Delta mntR$ mutant (Table 1), suggesting that Dpr and redox system proteins might play the major role in protecting *S. oligofermentans* from challenge with a higher H$_2$O$_2$ concentration.

Next, the role of Dpr and redox system proteins in the H$_2$O$_2$ resistance of *S. oligofermentans* was determined. The *tpx*, *trx*, *dpr*, and *mntABC* genes were each deleted, and the mutants were compared with the wild-type strain for growth suppression by 40 and 100 μM H$_2$O$_2$. As shown in Fig. 6, 100 μM H$_2$O$_2$ slightly suppressed the growth of the wild-type strain, but 40 μM H$_2$O$_2$ already retarded the growth of the
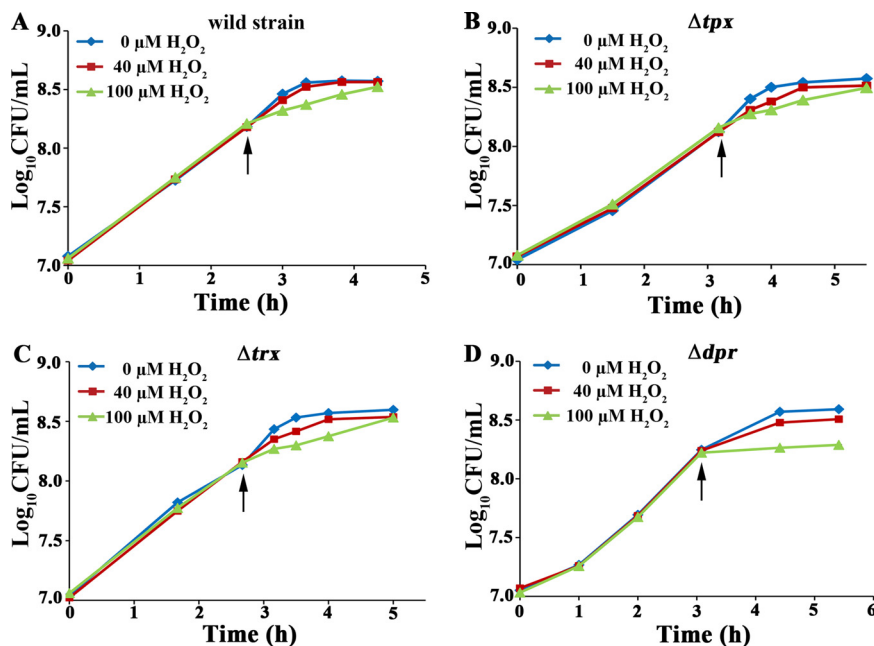

FIG 6 H$_2$O$_2$ sensitivity assay of mutants with deletions of the genes involved in cellular redox and metal homeostasis. Overnight cultures of the tested strains were diluted 1:30 into fresh BHI broth and anaerobically cultured. Triplicate cultures were used for each strain. When the OD$_{600}$ reached approximately 0.5, one replicate was left as the H$_2$O$_2$-untreated control and the other two were supplemented with 40 and 100 μM H$_2$O$_2$, respectively. The growth profiles of the tested strains were monitored by counting the number of CFU at the indicated time points. The experiments were repeated three times, with triplicate cultures being used each time. The averages from three independent experiments are shown. Black arrows indicate the time point of H$_2$O$_2$ supplementation.
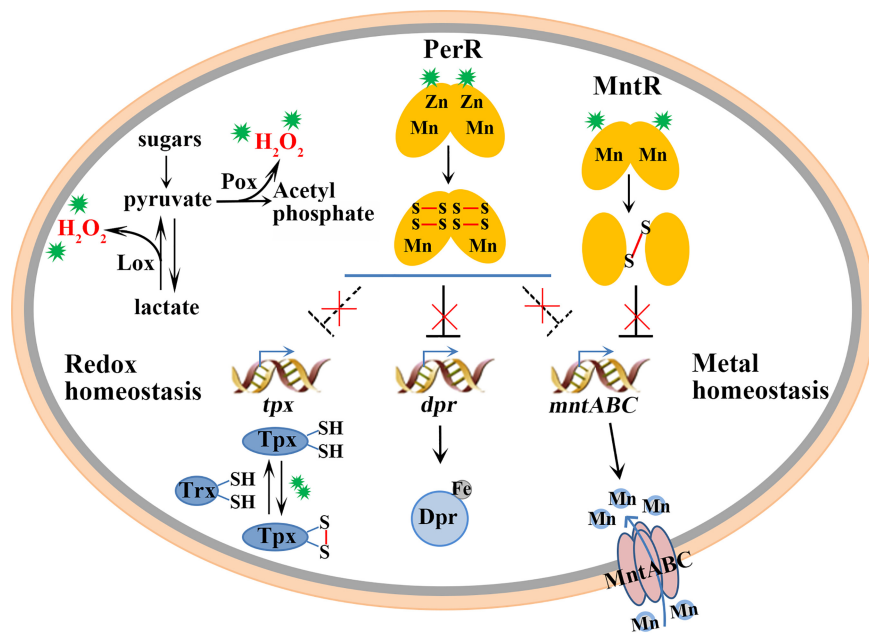
FIG 7 Diagram depicting the low-H_2O_2-concentration-induced adaptive mechanism against higher H_2O_2 stress in streptococci. The catalase-void streptococci use pyruvate oxidase (Pox) and lactate oxidase (Lox) to generate low levels of endogenous H_2O_2, which induces an adaptation to avoid attack by a higher H_2O_2 concentration. Redox proteomics analysis and physiological and genetic experiments identified a hierarchal H_2O_2-sensing and resistance network consisting of the H_2O_2-sensitive cysteine-containing proteins. These include redox transcriptional regulators, e.g., the peroxide response repressor PerR and the metalloregulator MntR, a repressor of the Mn^{2+} uptake regulon *mntABC*, as well as the redox homeostatic proteins, e.g., thiol peroxidase (Tpx), which catalyzes the reduction of H_2O_2, and thioredoxin (Trx), which specifically reduces H_2O_2 oxidation-generated disulfide linkages. Inactivation of PerR by trace H_2O_2 derepresses *tpx* and the genes encoding metal ion homeostatic proteins, like *mntR*, *dpr*, and *mntABC*, whereas oxidation inactivation of MntR derepresses *mntABC* (25). Dpr chelates free ferrous ion to avoid Fenton chemistry, whereas MntABC imports Mn^{2+} to decompose the cellular H_2O_2. These functional proteins help *S. oligofermentans* resist the stress associated with a higher H_2O_2 concentration. Of note, PerR directly represses the *dpr* gene and controls the *tpx*, *mntABC*, and *mntR* genes indirectly by unknown mechanisms. H_2O_2 is identified by the green symbols.

tpx, *trx*, and *dpr* deletion mutants, with the Δ*dpr* mutant being the most severely inhibited. The Δ*mntABC* mutant was reported to exhibit reduced resistance to 10 mM H_2O_2 (11), but its growth was not significantly inhibited by 100 μM H_2O_2 (data not shown). Collectively, the results indicate that the redox regulators PerR and MntR and their regulated cellular redox and metal homeostasis proteins are involved in the self-protection of *S. oligofermentans* from H_2O_2 stress.

DISCUSSION

Although a few studies have reported that endogenous H_2O_2 protects streptococci from challenge with a higher H_2O_2 concentration (8, 22), the mechanism remains unclear. In the present study, through a combination of physiological, biochemical, genetic, and redox proteomic studies, we elucidated the mechanism underlying the low-H_2O_2-concentration-induced adaptation of catalase-negative streptococci to a higher H_2O_2 concentration. Figure 7 depicts that streptococci employ pyruvate oxidase (Pox) and lactate oxidase (Lox) to produce endogenous H_2O_2. Two H_2O_2-sensing redox regulators, the peroxide-responsive repressor PerR and the metalloregulator MntR, are inactivated by H_2O_2 oxidation of the cysteine residues. PerR cysteine oxidation results in Zn^{2+} loss and the subsequent derepression of *dpr*, *mntABC*, *tpx*, and *mntR*. H_2O_2 oxidation of MntR leads to disulfide-linked intermolecular polymers and inactivates the regulator, thus derepressing the manganese uptake regulon *mntABC* (25). In addition to *dpr* and *mntABC*, as indicated in our previous work (11), *mntR* and the thiol peroxidase-encoding gene *tpx* were identified to be the PerR regulons. Deletion of these functional genes as well as the redox circuit protein Trx increased the sensitivity of *S. oligofer-*

mentans to a low H_2O_2 concentration, and correspondingly, deletion of either *mntR* or *perR* resulted in the streptococci becoming constitutively resistant to a higher H_2O_2 concentration. Thus, this work reveals a redox-regulated anti-H_2O_2 defense network, in which PerR has evolved to sense H_2O_2 by a Cys-based redox reaction in the manganese-rich cellular environments of the catalase-negative streptococci.

Cysteine residues are the most sensitive to H_2O_2 oxidation (41), and therefore, reversibly oxidized cysteine thiol modifications, such as SOH and the disulfide bond, usually function in the activation of redox regulatory proteins. Some redox regulators, such as the *E. coli* chaperone protein Hsp33 (37) and the *Streptomyces coelicolor* anti-sigma factor RsrA (38) and Fur-like repressor CatR (42), possess a structural Cys_4Zn. The Zn^{2+} at the Cys_4Zn site stabilizes the cysteine residues as thiolate, which may increase the reactivity of cysteine toward electrophilic H_2O_2 (43). The *S. oligofermentans* PerR possesses the structural Cys_4Zn as well. Redox proteomics, redox Western blotting, and LC-MS/MS identification of the immunoprecipitated protein all demonstrated that the cysteine residues of the streptococcal PerR are oxidized by a low H_2O_2 concentration (Fig. 4). Oxidation of the cysteine residues causes Zn^{2+} loss and inactivates PerR (Fig. 5), thereby derepressing the antioxidative genes (Table 3). This explains the underlying mechanism of the PerR-mediated H_2O_2 adaptation of streptococci.

It has been reported that the *B. subtilis* PerR, an ortholog of the streptococcal PerR (see Fig. S5 in the supplemental material), is inactivated by histidine oxidation, whereas its Zn^{2+}-coordinated cysteine residues are inert to H_2O_2 oxidation (20). In contrast, the streptococcal PerR is inactivated by H_2O_2 oxidation at the Zn^{2+}-coordinated cysteine residues (Fig. 4 and 5). Subsequent structural homology modeling of the *S. oligofermentans* PerR was performed with the SWISS-MODEL server by automatically selecting the *S. pyogenes* PerR (PDB accession number 4LMY) as a template. Structural comparison with *B. subtilis* PerR (PDB accession number 2FE3) did show some differences between the two at the C-terminal Cys_4Zn site (Fig. S5); specifically, Cys103 and Cys142 of the *S. oligofermentans* PerR are situated close to the N terminus of the S4 β-strand and at a short H6 helix, respectively, while Cys96 and Cys139 of the *B. subtilis* PerR are situated at the C terminus of the S3 β-strand and in the center of a long H6 helix, respectively. These differences may render the two PerRs with different H_2O_2 sensitivities, as a cysteine residue near the N terminus of a helix more likely possesses lower pK_a values (43). Cellular metal environments could be another clue to the distinct inactivation mechanisms of the two PerRs. A much higher ratio of Mn/Fe was determined in *S. oligofermentans* cells (1.02 ± 0.25) than in *B. subtilis* cells (0.05 ± 0.01), which was paralleled in this study, in accordance with the Mn-centric definition of streptococci (44–46). Especially, when grown in a medium supplemented with 2.5 μM and 100 μM Mn^{2+}, 1.78 ± 0.46 and 8.04 ± 0.42 cellular Mn/Fe ratios were found in *S. oligofermentans*, respectively (25), indicating an active manganese uptake system in this bacterium. The higher cellular Mn/Fe ratio in streptococci could result in higher percentages of PerR:Zn,Mn than of the PerR:Zn,Fe found in bacilli; thus, cysteine oxidation contributes to H_2O_2 inactivation of the streptococcal PerR:Zn,Mn proteins (Fig. 4 and 5; Table S1). Nevertheless, the possibility of Fe^{2+}-triggered streptococcal PerR inactivation cannot be excluded, as approximately 28% of His40 residues and 53% of His95 residues in PerR were oxidized when *S. oligofermentans* was grown in BHI broth containing 0.5 μM Mn^{2+} and 15 μM Fe^{2+} (Table S1). Therefore, the dual-H_2O_2-sensing mechanisms of the redox regulator PerR could provide protection for the catalase-negative streptococci from oxidative stress in environments with different metal ions.

Metal homeostasis plays a central role in oxidative stress resistance in Gram-positive bacteria (4, 44, 47, 48). In addition to PerR, streptococci also employ MntR, a metalloregulator protein, to control cellular manganese and iron homeostasis (11, 16, 21, 25). Oxidative inactivation of PerR and MntR derepresses the expression of the metal homeostasis-related genes *dpr* and *mntABC* (Table 3) (25). Dpr chelates cellular Fe^{2+} and so prevents the production of highly toxic $HO·$, and the manganese importer MntABC takes up Mn^{2+} to decompose cellular H_2O_2. MntABC and Dpr have been verified to protect *S. oligofermentans* from challenge by a high H_2O_2 concentration in

our previous studies (11). Here, Dpr was further verified to resist a sublethal H_2O_2 concentration.

The thioredoxin (Trx) system, which is comprised of NADPH, thioredoxin reductase (TrxR), and thioredoxin, plays a key role in defense against oxidative stress, particularly in the catalase-lacking streptococci (9, 49–51). Oxidation of the cysteine thiol groups of Trx and Tpx has been found in 40 μM H_2O_2-pretreated *S. oligofermentans* cells (Fig. 3), and deletion of two genes increases the H_2O_2 sensitivity of the streptococcus (Fig. 6). This observation indicates that the Trx system is involved in the H_2O_2 adaptation of *S. oligofermentans*, which is presumably under the control of PerR.

In conclusion, this work reports a novel H_2O_2 adaptation mechanism. Trace amounts of cellular H_2O_2 cause thiol oxidation of the redox-based regulatory and functional proteins and activate antioxidative systems; meanwhile, they reduce the level of glycolysis, which generates ROS precursors. This H_2O_2 adaptation mechanism could be an important antioxidative defense strategy of the catalase-void anaerobes.

MATERIALS AND METHODS

Bacterial strains and culture conditions. *S. oligofermentans* AS 1.3089 (52) and its derivative strains (see Table S3 in the supplemental material) were grown in brain heart infusion (BHI) broth (BD Difco, Franklin Lakes, NJ) statically or anaerobically under 100% N_2. *Escherichia coli* DH5α, used for cloning, was grown in Luria-Bertani (LB) broth at 37°C under shaking. When required, kanamycin (1 mg/ml) and spectinomycin (1 mg/ml) were used for the selection of *Streptococcus* transformants, while ampicillin (100 μg/ml) and spectinomycin (250 μg/ml) were used to select *E. coli* transformants.

Construction of genetically altered strains. All primers used in this study are listed in Table S3. *tpx*, *trx*, *dpr*, and *perR* deletion strains were constructed using the PCR-ligation method (53). The upstream and downstream DNA fragments of each gene were amplified from the genomic DNA. The purified, BamHI-digested PCR products were ligated with a kanamycin resistance gene fragment from plasmid pALH124 (54) or a spectinomycin resistance gene fragment from pDL278 (55) at compatible sites. For construction of 6×His-tagged strains, the *tpx*, *trx*, and *perR* genes were amplified from the genomic DNA using a pair of primers, with the reverse primer carrying a sequence encoding 6 histidines just before the termination codon. Meanwhile, an ~600-bp DNA fragment immediately downstream of the termination codon of each gene was amplified. The purified PCR products were digested with BamHI and ligated with the kanamycin resistance gene fragment. The ligation mixtures were transformed into the *S. oligofermentans* wild-type strain, except that the ligation mixture for *perR* deletion was transformed into the Δ*mntR* strain (11) to construct a Δ*perR* Δ*mntR* strain, as described previously (6). For construction of the *perR*::pDL278-*perR*C139S-6×His and *perR*::pDL278-*perR*C142S-6×His strains, the *perR*-6×His gene fusion was amplified from the genomic DNA of the strain with 6×His-tagged PerR. After digestion with EcoRI and SalI, the purified product was inserted into the compatible sites on the *E. coli*-streptococci shuttle vector pDL278 (55) to produce pDL278-*perR*-6×His. Then, Cys139 and Cys142 were mutated into serine using a site-directed gene mutagenesis kit (Beyotime Biotechnology Co., Shanghai, China). The correct pDL278-*perR*-6×His, pDL278-*perR*C139S-6×His, and pDL278-*perR*C142S-6×His plasmids were transformed into the *perR* deletion strain to produce strains ectopically expressing wild-type and cysteine-mutated *perR*.

Detection of intracellular hydrogen peroxide by HyPer imaging. Mid-exponential-phase HyPer reporter cells were pelleted, washed twice with phosphate-buffered saline (PBS), resuspended in 100 μl of PBS, and exposed to air in the dark for 30 min. Forty microliters of cells was placed on a Polysine microscope slide (25 by 75 by 1 mm; Thermo Scientific, Waltham, MA), covered with a Fisher-brand microscope glass coverslip (diameter, 15 mm; thickness, 0.13 to 0.17 mm; Thermo Scientific), and then visualized under a confocal laser scanning microscope (Leica model TCS SP8; Leica Microsystems, Buffalo Grove, IL, USA). Excitation was provided at 488 nm, with emission being collected from a wavelength range of 500 to 530 nm (32, 56). For each sample, at least 5 fluorescent and differential interference contrast (DIC) images were captured. The fluorescence intensities of 25 regions of interest (ROI), with each ROI containing 5 cells, from each sample were measured using Leica Application Suite (LAS) AF software. For images with fluorescence that was too weak, the ROI in the corresponding DIC images was framed, and the fluorescence was measured in the same ROI in the fluorescence image. The average fluorescence intensities of 25 ROIs were calculated and are expressed in arbitrary units (a.u.) per ROI ± standard deviation.

Redox proteomics analysis by differential alkylation and LC-MS/MS. The differential alkylation method (34) was used to identify H_2O_2-induced changes in the thiol redox status of the proteins. Briefly, mid-exponential-phase cells in the tested samples were collected by centrifugation and resuspended in radioimmunoprecipitation assay (RIPA) buffer (50 mM Tris [pH 7.4], 150 mM NaCl, 1% Triton X-100, 1% sodium deoxycholate, 0.1% SDS, 2 mM sodium pyrophosphate, 25 mM β-glycerophosphate, 1 mM sodium orthovanadate, sodium fluoride, 1 mM EDTA, 0.5 μg/ml leupeptin) containing 1 mM phenylmethylsulfonyl fluoride (PMSF). To minimize an artificial oxidation during sample preparation, cell breakage by sonication was performed inside an anaerobic chamber (Thermo Scientific); moreover, 10 mM EDTA and 1 kU/ml catalase were included in the lysis buffer to prevent an Fe^{2+}-triggered Fenton reaction and decompose H_2O_2, respectively. The sonication was implemented on ice in the dark using a UP-400S

ultrasonicator (Xinzi Company, Ningbo, China), and cell lysates were centrifuged at 8,000 × g for 15 min, and then the protein concentration in the supernatant was measured using a Pierce bicinchoninic acid (BCA) protein assay kit (Thermo Scientific). The same amounts of protein from all the samples were separated on a nonreducing one-dimensional SDS-PAGE gel, and each gel lane was cut into 6 slices and washed with MS-grade water three times. The proteins in the gel were alkylated for 30 min with 55 mM [^{13}C]iodoacetic acid in 50 mM NH$_4$HCO$_3$ (pH 8.0) in the dark. After removing the iodoacetic acid, 25 mM DTT reduction was performed for 45 min at 55°C, and then the DTT was removed and the proteins were alkylated with 55 mM [^{12}C]iodoacetic acid for 30 min in the dark. Upon in-gel digestion with MS-grade trypsin (Promega, Fitchburg, WI), LC-MS/MS analysis was implemented with an Easy-nLC integrated nano-high-performance liquid chromatography system (Proxeon, Odense, Denmark) and a Q-Extractive mass spectrometer (Thermo Scientific, Waltham, MA), as described previously (28).

MS/MS spectra were searched against the forward and reverse *S. oligofermentans* protein database, downloaded from UniProt, using the SEQUEST search engine of Proteome Discoverer software (v1.4). The precursor ion mass tolerance was 20 ppm for all mass spectra acquired in an Orbitrap mass analyzer, and the fragment ion mass tolerance was 0.02 Da for all MS/MS spectra. The following search criteria were employed: full tryptic specificity was required; two missed cleavages were allowed; ^{13}C carboxymethylation (free cysteine residue), ^{12}C carboxymethylation (disulfide linkage cysteine residue) and sulfenic, sulfinic, and sulfonic acids were variable modifications for cysteine; oxidation was a variable modification for methionine; and the false discovery rate (FDR) was set to 0.01. All the cysteine-modified MS/MS spectra were manually confirmed. The MaxQuant software package was used to obtain the intensity of the cysteine-modified peptides. Duplicate experiments were performed in parallel.

Protein GO category analysis. Homologues of the *S. oligofermentans* redox-sensitive proteins were searched for in *S. pneumoniae* and put into the PANTHER bioinformatics platform (http://www.pantherdb .org/) for Gene Ontology (GO) analysis. GO enrichment analysis was implemented on the Gene Ontology Consortium website (http://www.geneontology.org), the binomial test was used for analysis of statistical significance, and a P value of <0.05 was used as a cutoff.

Redox Western blotting. Cells were collected by centrifugation and resuspended in RIPA buffer (50 mM Tris-HCl, pH 7.4, 150 mM NaCl, 1% Triton X-100, 1% sodium deoxycholate, 0.1% SDS, sodium orthovanadate, sodium fluoride, EDTA, leupeptin) with addition of 40 mM N-ethylmaleimide (NEM), 1 mM PMSF, 10 mM EDTA, and 1 kU/ml catalase. Cells were sonicated on ice in the dark for 45 min and alkylated in the dark for 20 min, and then the supernatant were collected by centrifugation. Reduced samples were prepared by incubating the lysates with 50 mM DTT for 1 h. For the 4-acetamido-4′-maleimidylstilbene-2,2′-disulfonic acid (AMS) alkylating experiment, cells were resuspended in PBS buffer containing 15 mM AMS, 1 mM PMSF, 10 mM EDTA, and 1 kU/ml catalase, sonicated, and then incubated at 4°C for 2 h in the dark. Half of the samples were reduced with 50 mM DTT for 1 h, and then the DTT was removed and the samples were alkylated with 15 mM AMS at 4°C for 2 h in the dark. The protein concentration of the lysate was determined using a BCA protein assay kit. Protein samples were diluted in nonreducing loading buffer (4×; 0.2 M Tris-HCl, pH 6.8, 40% glycerol, 8% SDS, 0.4% bromphenol blue), separated by SDS-PAGE, transferred onto a nitrocellulose membrane, and hybridized with an anti-His tag antibody (Abmart Company, Shanghai, China) at a 4,000-fold dilution. Detection was performed using a chemiluminescent nucleic acid detection module kit (Thermo Scientific).

IP and LC-MS/MS identification of cysteine thiol oxidation of the PerR protein *in vivo*. 6×His-tagged PerR protein was purified by immunoprecipitation (IP) using anti-His tag monoclonal antibody-magnetic agarose (MBL International Corporation, Woburn, MA) according to the instructions of the manufacturer. Briefly, the 6×His-tagged-PerR-expressing strain PerR-6×His was statically grown in BHI broth. The mid-exponential-phase cells were collected and washed with PBS three times. Then, the cells were resuspended in lysis buffer (50 mM Tris-HCl, 150 mM NaCl, 0.05% NP-40, 1 mM DTT) containing 55 mM [^{13}C]iodoacetic acid, 10 mM EDTA and 1 kU/ml catalase. The cells were sonicated on ice in the dark for 45 min and alkylated in the dark for 20 min, and then the cell lysate was subjected to centrifugation. The obtained supernatant was mixed and incubated with the magnetic beads. After washing 4 times with lysis buffer, the immunoprecipitated 6×His-tagged PerR protein was eluted by boiling in nonreducing SDS sample buffer (4% SDS, 125 mM Tris-HCl, pH 8.0, 20% glycerol) and separated using 18% nonreducing SDS-PAGE. The target PerR protein band with the expected molecular size was cut from the gel, and cysteine residue oxidation was identified by differential alkylation and LC-MS/MS, as described above, except that the reduced and oxidized cysteine residues were alkylated with 55 mM [^{13}C]iodoacetic acid and [^{12}C]iodoacetamide, respectively.

Overexpression of PerR-GST, Tpx-6×His, and Trx-6×His proteins. A 450-bp DNA fragment containing the entire *perR* coding gene was PCR amplified. The purified PCR product was digested with EcoRI/XhoI and ligated into the compatible sites on pGEX4T-1 (GE Healthcare, Boston, MA), and the produced pGEX-PerR was transformed into *E. coli* BL21(DE3) cells (Novagen, Madison, WI). Correct transformants were grown at 37°C to an OD$_{600}$ of 0.4 to 0.6, and 0.1 mM isopropyl-β-D-thiogalactopyranoside (IPTG; Sigma-Aldrich, St. Louis, MO) was added to induce PerR-GST expression at 22°C overnight. Then, the cells were collected by centrifugation and resuspended in phosphate-buffered saline (PBS; 10 mM Na$_2$HPO$_4$, 1.8 mM KH$_2$PO$_4$, 137 mM NaCl, 2.7 mM KCl, pH 7.4) containing 1 mM DTT and 10 mM EDTA and then lysed by sonication for 30 min. The cell lysate was centrifuged at 8,000 × g for 30 min, and the supernatant was filtered through a 0.22-nm-pore-size polyvinylidene difluoride membrane (Millipore, Billerica, MA) and then applied to a GSTrap HP column (GE Healthcare, Boston, MA). The proteins were eluted with elution buffer (20 mM Tris-HCl buffer containing 1 mM DTT, 10 mM EDTA, and 10 mM reduced glutathione [GSH], pH 8.0), and the elution fractions were analyzed by electrophoresis on a 12% SDS-PAGE gel. The fractions with the desired protein were pooled and dialyzed against

PBS buffer containing 3 mM GSH and 10 mM EDTA three times. Then, the purified proteins were stored in aliquots in 10% glycerol at −80°C until use.

For the overexpression of the Tpx-6×His and Trx-6×His proteins, 492- and 552-bp DNA fragments containing the entire *tpx* and *trx* coding genes, respectively, were PCR amplified with the primer pairs listed in Table S3. The resultant products were integrated into pET-28a (Novagen, Madison, WI) by Gibson assembly (New England Biolabs, Beverly, MA) to produce pET-28a-Tpx and pET-28a-Trx. The correct constructs were transformed into *E. coli* BL21(DE3) (Novagen, Madison, WI) cells. Correct transformants were grown at 37°C to an OD_{600} of 0.6 to 0.8, 0.1 mM IPTG (Sigma-Aldrich, St. Louis, MO) was added, and the cells were incubated at 22°C overnight. Then, the cells were collected by centrifugation, resuspended in binding buffer (20 mM sodium phosphate, 500 mM NaCl, 30 mM imidazole, 1 mM EDTA, 1 mM DTT, pH 7.4), and lysed by sonication for 30 min. The supernatant was filtered and then applied to an Ni^{2+}-charged chelating column (GE Healthcare, Piscataway, NJ) that had previously been equilibrated with binding buffer. Proteins were eluted with elution buffer (20 mM sodium phosphate, 500 mM NaCl, 500 mM imidazole, 1 mM DTT, pH 7.4). The fractions with the desired protein were pooled and dialyzed against buffer containing 20 mM Tris-HCl, 150 mM NaCl, 1 mM DTT, and 1 mM EDTA. The purified Tpx-6×His and Trx-6×His proteins were stored in aliquots in 10% glycerol at −80°C until use.

Nonreducing SDS-PAGE. Five micrograms of PerR-GST protein was treated or not treated with 5 mM H_2O_2 for 30 min and with or without a subsequent reduction by 50 mM DTT for 1 h. Before electrophoresis, 40 mM NEM was added, and the mixture was kept in the dark for 30 min. The protein samples were diluted in nonreducing SDS loading buffer (4×; 0.2 M Tris-HCl, pH 6.8, 40% glycerol, 8% SDS, 0.4% bromphenol blue) and then separated on a 12% SDS-PAGE gel.

Determination of zinc content in PerR-GST using ICP-MS. The PerR-GST protein was treated or not treated with 5 mM H_2O_2 for 30 min and with or without a subsequent reduction by 50 mM DTT for 1 h and was then transferred into Chelex 100-treated PBS buffer via ultrafiltration. Protein concentrations were measured with a BCA protein assay kit. The protein samples were treated with nitric acid (ultrapure), and then the zinc content was analyzed by inductively coupled plasma mass spectrometry (ICP-MS; DRCII apparatus; PerkinElmer, USA) at Peking University Health Science Center. Beryllium, indium, and uranium standard solutions (NIST certified; PerkinElmer) were used to calibrate the ICP-MS. Experiments were conducted for triplicate samples and repeated at least three times.

Electrophoretic mobility shift assay (EMSA). The target gene promoter fragments were generated by PCR amplification using the biotin-labeled primer pair listed in Table S3. The PerR-GST protein was first dialyzed into PBS buffer containing 10 mM EDTA and 1 mM DTT and then digested with 100 U thrombin to remove the GST tag. One micromole of the PerR protein was preincubated with 1 mM $MnCl_2$, and then 0.2 nM a biotin-labeled double-stranded DNA probe and increasing amounts of PerR (0 to 200 nM) were mixed in the binding buffer [10 mM Tris-HCl, pH 8.0, 5% glycerol, 50 mM NaCl, 10 μg/ml bovine serum albumin, 2 ng/μl poly(dl·dC), 0.5 mM DTT, 1 mM $MnCl_2$]. The reaction proceeded at 30°C for 30 min. To observe the effect of H_2O_2 on PerR binding, 1 μM PerR protein was preincubated with 1 mM $MnCl_2$ and then treated with various concentrations of H_2O_2 (0 to 200 μM) at 30°C for 30 min or with 200 μM H_2O_2 at 30°C for various times (0 to 30 min), and then catalase was added to a final concentration of 150 U/ml and the mixture was incubated at 37°C for 30 min. To determine whether oxidation was reversible, 10 mM DTT was added to reduce the 200 μM H_2O_2-treated PerR at 37°C for 1 h. Then, 50 nM H_2O_2-oxidized or DTT-reduced PerR protein was tested for binding to a 0.2 nM biotin-labeled *dpr* promoter fragment. The binding mixtures were electrophoresed on a 6% polyacrylamide gel on ice. The DNA-protein complex was transferred onto a nylon membrane and detected with a chemiluminescent nucleic acid detection module kit (Thermo Scientific).

Determination of H_2O_2 survival rate. Overnight cultures of the tested strains were diluted 1:30 into fresh BHI broth and incubated strictly anaerobically. When the OD_{600} reached 0.4 to 0.5, the cells were separated into three aliquots. One aliquot was treated with 10 mM H_2O_2 for 10 min, and another was prepulsed with 40 μM H_2O_2 for 20 min before being subjected to 10 mM H_2O_2 treatment, while an aliquot not treated with 10 mM H_2O_2 was used as a control. Then, the cells were collected, washed twice with PBS, and resuspended in 200 μl BHI broth. Cell chains were separated by sonication for 30 s with an XC-3200D ultrasonic cleaner (Xinchen Company, Nanjing, China), and then 10-fold serial dilutions were performed. Appropriate dilutions were plated on BHI agar plates, and the numbers of CFU were counted after 24 h of incubation in a candle jar at 37°C. The survival percentage was calculated by dividing the number of CFU of the H_2O_2-challenged sample by the number of CFU of the corresponding controls. Experiments were executed in triplicate, and each experiment was repeated at least three times independently.

Assay of growth under H_2O_2 stress. *S. oligofermentans* wild-type and gene deletion strains were grown anaerobically in BHI broth until the OD_{600} reached ∼0.5, with three replicates of each strain being included. Two replicate cultures were supplemented with 40 and 100 μM H_2O_2, respectively, leaving one replicate as an H_2O_2-untreated control. The growth profiles were measured by counting the number of CFU at the different time intervals. Triplicates for each sample were measured, and the experiments were repeated at least three times.

Determination of excreted hydrogen peroxide in culture. The hydrogen peroxide in the culture suspension was quantified as described previously (11). Briefly, 650 μl of culture supernatant was added to 600 μl of a solution containing 2.5 mM 4-amino-antipyrine (4-amino-2,3-dimethyl-1-phenyl-3-pyrazolin-5-one) (Sigma-Aldrich) and 0.17 M phenol. The reaction proceeded for 4 min at room temperature; horseradish peroxidase (Sigma-Aldrich) was then added to a final concentration of 50 mU/ml in 0.2 M potassium phosphate buffer (pH 7.2). After 4 min of incubation at room temperature, the optical

density at 510 nm was measured with a Unico 2100 visible spectrophotometer (Unico, Shanghai, China). A standard curve was generated with known concentrations of chemical H$_2$O$_2$.

Quantitative PCR. Total RNA was extracted from mid-exponential-phase (OD$_{600}$, ~0.4 to 0.5) H$_2$O$_2$-treated and -untreated *S. oligofermentans* cells using the TRIzol reagent (Invitrogen, Carlsbad, CA), as recommended by the supplier. After quality confirmation with a 1% agarose gel, the RNA was treated with RNase-free DNase (Promega, Madison, WI) and analyzed by PCR for possible chromosomal DNA contamination. cDNA was generated from 2 μg total RNA with random primers using Moloney murine leukemia virus reverse transcriptase (Promega, Madison, WI), according to the supplier's instructions, and was used for quantitative PCR (qPCR) amplification with the corresponding primers (Table S3). Amplifications were performed with a Mastercycler ep realplex^2 instrument (Eppendorf, Germany). To estimate the copy numbers of the tested genes, a standard curve for each tested gene was generated by quantitative PCR using a 10-fold serially diluted PCR product as the template. The 16S rRNA gene was used as the biomass reference. The number of copies of the tested gene transcript per 100 16S rRNA copies is shown. All measurements were done for triplicate samples, and the experiments were repeated at least three times.

SUPPLEMENTAL MATERIAL

Supplemental material is available online only.

FIG S1, TIF file, 2 MB.
FIG S2, TIF file, 0.2 MB.
FIG S3, TIF file, 0.1 MB.
FIG S4, TIF file, 0.6 MB.
FIG S5, TIF file, 2.1 MB.
TABLE S1, DOCX file, 0.02 MB.
TABLE S2, DOCX file, 0.02 MB.
TABLE S3, DOCX file, 0.02 MB.
DATA SET S1, XLSX file, 0.3 MB.
DATA SET S2, XLSX file, 0.3 MB.

ACKNOWLEDGMENT

REFERENCES

1. Miller RA, Britigan BE. 1997. Role of oxidants in microbial pathophysiology. Clin Microbiol Rev 10:1–18. https://doi.org/10.1128/CMR.10.1.1.
2. Winterbourn CC, Kettle AJ, Hampton MB. 2016. Reactive oxygen species and neutrophil function. Annu Rev Biochem 85:765–792. https://doi.org/10.1146/annurev-biochem-060815-014442.
3. Imlay JA. 2013. The molecular mechanisms and physiological consequences of oxidative stress: lessons from a model bacterium. Nat Rev Microbiol 11:443–454. https://doi.org/10.1038/nrmicro3032.
4. Faulkner MJ, Helmann JD. 2011. Peroxide stress elicits adaptive changes in bacterial metal ion homeostasis. Antioxid Redox Signal 15:175–189. https://doi.org/10.1089/ars.2010.3682.
5. Liu L, Tong H, Dong X. 2012. Function of the pyruvate oxidase-lactate oxidase cascade in interspecies competition between *Streptococcus oligofermentans* and *Streptococcus mutans*. Appl Environ Microbiol 78:2120–2127. https://doi.org/10.1128/AEM.07539-11.
6. Tong H, Chen W, Merritt J, Qi F, Shi W, Dong X. 2007. *Streptococcus oligofermentans* inhibits *Streptococcus mutans* through conversion of lactic acid into inhibitory H$_2$O$_2$: a possible counteroffensive strategy for interspecies competition. Mol Microbiol 63:872–880. https://doi.org/10.1111/j.1365-2958.2006.05546.x.
7. Tong H, Chen W, Shi W, Qi F, Dong X. 2008. SO-LAAO, a novel L-amino acid oxidase that enables *Streptococcus oligofermentans* to outcompete *Streptococcus mutans* by generating H$_2$O$_2$ from peptone. J Bacteriol 190:4716–4721. https://doi.org/10.1128/JB.00363-08.
8. Lisher JP, Tsui HT, Ramos-Montanez S, Hentchel KL, Martin JE, Trinidad JC, Winkler ME, Giedroc DP. 2017. Biological and chemical adaptation to endogenous hydrogen peroxide production in *Streptococcus pneumoniae* D39. mSphere 2:e00291-16. https://doi.org/10.1128/mSphere.00291-16.
9. Henningham A, Dohrmann S, Nizet V, Cole JN. 2015. Mechanisms of group A *Streptococcus* resistance to reactive oxygen species. FEMS Microbiol Rev 39:488–508. https://doi.org/10.1093/femsre/fuu009.
10. Yesilkaya H, Andisi VF, Andrew PW, Bijlsma JJ. 2013. *Streptococcus pneumoniae* and reactive oxygen species: an unusual approach to living with radicals. Trends Microbiol 21:187–195. https://doi.org/10.1016/j.tim.2013.01.004.
11. Wang X, Tong H, Dong X. 2014. PerR-regulated manganese ion uptake contributes to oxidative stress defense in an oral streptococcus. Appl Environ Microbiol 80:2351–2359. https://doi.org/10.1128/AEM.00064-14.
12. Hillion M, Antelmann H. 2015. Thiol-based redox switches in prokaryotes. Biol Chem 396:415–444. https://doi.org/10.1515/hsz-2015-0102.
13. Antelmann H, Helmann JD. 2011. Thiol-based redox switches and gene regulation. Antioxid Redox Signal 14:1049–1063. https://doi.org/10.1089/ars.2010.3400.
14. Marinho HS, Real C, Cyrne L, Soares H, Antunes F. 2014. Hydrogen peroxide sensing, signaling and regulation of transcription factors. Redox Biol 2:535–562. https://doi.org/10.1016/j.redox.2014.02.006.
15. Zheng M, Aslund F, Storz G. 1998. Activation of the OxyR transcription factor by reversible disulfide bond formation. Science 279:1718–1721. https://doi.org/10.1126/science.279.5357.1718.
16. Turner AG, Ong CY, Djoko KY, West NP, Davies MR, McEwan AG, Walker MJ. 2017. The PerR-regulated P$_{1B-4}$-type ATPase (PmtA) acts as a ferrous iron efflux pump in *Streptococcus pyogenes*. Infect Immun 85:e00140-17. https://doi.org/10.1128/IAI.00140-17.
17. Fuangthong M, Herbig AF, Bsat N, Helmann JD. 2002. Regulation of the *Bacillus subtilis fur* and *perR* genes by PerR: not all members of the PerR regulon are peroxide inducible. J Bacteriol 184:3276–3286. https://doi.org/10.1128/jb.184.12.3276-3286.2002.
18. Jacquamet L, Traore DA, Ferrer JL, Proux O, Testemale D, Hazemann JL, Nazarenko E, El Ghazouani A, Caux-Thang C, Duarte V, Latour JM. 2009. Structural characterization of the active form of PerR: insights into the metal-induced activation of PerR and Fur proteins for DNA binding. Mol Microbiol 73:20–31. https://doi.org/10.1111/j.1365-2958.2009.06753.x.

19. Herbig AF, Helmann JD. 2001. Roles of metal ions and hydrogen peroxide in modulating the interaction of the *Bacillus subtilis* PerR peroxide regulon repressor with operator DNA. Mol Microbiol 41:849–859. https://doi.org/10.1046/j.1365-2958.2001.02543.x.

20. Lee JW, Helmann JD. 2006. The PerR transcription factor senses H_2O_2 by metal-catalysed histidine oxidation. Nature 440:363–367. https://doi.org/10.1038/nature04537.

21. Makthal N, Rastegari S, Sanson M, Ma Z, Olsen RJ, Helmann JD, Musser JM, Kumaraswami M. 2013. Crystal structure of peroxide stress regulator from *Streptococcus pyogenes* provides functional insights into the mechanism of oxidative stress sensing. J Biol Chem 288:18311–18324. https://doi.org/10.1074/jbc.M113.456590.

22. Grifantini R, Toukoki C, Colaprico A, Gryllos I. 2011. Peroxide stimulon and role of PerR in group A *Streptococcus*. J Bacteriol 193:6539–6551. https://doi.org/10.1128/JB.05924-11.

23. Rhee SG. 2006. Cell signaling. H_2O_2, a necessary evil for cell signaling. Science 312:1882–1883. https://doi.org/10.1126/science.1130481.

24. Sun F, Liang H, Kong X, Xie S, Cho H, Deng X, Ji Q, Zhang H, Alvarez S, Hicks LM, Bae T, Luo C, Jiang H, He C. 2012. Quorum-sensing agr mediates bacterial oxidation response via an intramolecular disulfide redox switch in the response regulator AgrA. Proc Natl Acad Sci U S A 109:9095–9100. https://doi.org/10.1073/pnas.1200603109.

25. Chen Z, Wang X, Yang F, Hu Q, Tong H, Dong X. 2017. Molecular insights into hydrogen peroxide-sensing mechanism of the metalloregulator MntR in controlling bacterial resistance to oxidative stresses. J Biol Chem 292:5519–5531. https://doi.org/10.1074/jbc.M116.764126.

26. Lindahl M, Mata-Cabana A, Kieselbach T. 2011. The disulfide proteome and other reactive cysteine proteomes: analysis and functional significance. Antioxid Redox Signal 14:2581–2642. https://doi.org/10.1089/ars.2010.3551.

27. Leonard SE, Carroll KS. 2011. Chemical 'omics' approaches for understanding protein cysteine oxidation in biology. Curr Opin Chem Biol 15:88–102. https://doi.org/10.1016/j.cbpa.2010.11.012.

28. Wang J, Jin L, Li X, Deng H, Chen Y, Lian Q, Ge R, Deng H. 2013. Gossypol induces apoptosis in ovarian cancer cells through oxidative stress. Mol Biosyst 9:1489–1497. https://doi.org/10.1039/c3mb25461e.

29. Leichert LI, Gehrke F, Gudiseva HV, Blackwell T, Ilbert M, Walker AK, Strahler JR, Andrews PC, Jakob U. 2008. Quantifying changes in the thiol redox proteome upon oxidative stress in vivo. Proc Natl Acad Sci U S A 105:8197–8202. https://doi.org/10.1073/pnas.0707723105.

30. Deng X, Weerapana E, Ulanovskaya O, Sun F, Liang H, Ji Q, Ye Y, Fu Y, Zhou L, Li J, Zhang H, Wang C, Alvarez S, Hicks LM, Lan L, Wu M, Cravatt BF, He C. 2013. Proteome-wide quantification and characterization of oxidation-sensitive cysteines in pathogenic bacteria. Cell Host Microbe 13:358–370. https://doi.org/10.1016/j.chom.2013.02.004.

31. Pericone CD, Park S, Imlay JA, Weiser JN. 2003. Factors contributing to hydrogen peroxide resistance in *Streptococcus pneumoniae* include pyruvate oxidase (SpxB) and avoidance of the toxic effects of the Fenton reaction. J Bacteriol 185:6815–6825. https://doi.org/10.1128/jb.185.23.6815-6825.2003.

32. Belousov VV, Fradkov AF, Lukyanov KA, Staroverov DB, Shakhbazov KS, Terskikh AV, Lukyanov S. 2006. Genetically encoded fluorescent indicator for intracellular hydrogen peroxide. Nat Methods 3:281–286. https://doi.org/10.1038/nmeth866.

33. Tong H, Wang X, Dong Y, Hu Q, Zhao Z, Zhu Y, Dong L, Bai F, Dong X. 2019. A *Streptococcus* aquaporin acts as peroxiporin for efflux of cellular hydrogen peroxide and alleviation of oxidative stress. J Biol Chem 294:4583–4595. https://doi.org/10.1074/jbc.RA118.006877.

34. Schilling B, Yoo CB, Collins CJ, Gibson BW. 2004. Determining cysteine oxidation status using differential alkylation. Int J Mass Spectrom 236:117–127. https://doi.org/10.1016/j.ijms.2004.06.004.

35. Mi H, Huang X, Muruganujan A, Tang H, Mills C, Kang D, Thomas PD. 2017. PANTHER version 11: expanded annotation data from Gene Ontology and Reactome pathways, and data analysis tool enhancements. Nucleic Acids Res 45:D183–D189. https://doi.org/10.1093/nar/gkw1138.

36. Hajaj B, Yesilkaya H, Benisty R, David M, Andrew PW, Porat N. 2012. Thiol peroxidase is an important component of *Streptococcus pneumoniae* in oxygenated environments. Infect Immun 80:4333–4343. https://doi.org/10.1128/IAI.00126-12.

37. Jakob U, Eser M, Bardwell JC. 2000. Redox switch of Hsp33 has a novel

zinc-binding motif. J Biol Chem 275:38302–38310. https://doi.org/10.1074/jbc.M005957200.

38. Bae JB, Park JH, Hahn MY, Kim MS, Roe JH. 2004. Redox-dependent changes in RsrA, an anti-sigma factor in *Streptomyces coelicolor*: zinc release and disulfide bond formation. J Mol Biol 335:425–435. https://doi.org/10.1016/j.jmb.2003.10.065.

39. Horsburgh MJ, Clements MO, Crossley H, Ingham E, Foster SJ. 2001. PerR controls oxidative stress resistance and iron storage proteins and is required for virulence in *Staphylococcus aureus*. Infect Immun 69:3744–3754. https://doi.org/10.1128/IAI.69.6.3744-3754.2001.

40. Hillmann F, Doring C, Riebe O, Ehrenreich A, Fischer RJ, Bahl H. 2009. The role of PerR in O_2-affected gene expression of *Clostridium acetobutylicum*. J Bacteriol 191:6082–6093. https://doi.org/10.1128/JB.00351-09.

41. Di Simplicio P, Franconi F, Frosali S, Di Giuseppe D. 2003. Thiolation and nitrosation of cysteines in biological fluids and cells. Amino Acids 25:323–339. https://doi.org/10.1007/s00726-003-0020-1.

42. Hahn JS, Oh SY, Chater KF, Cho YH, Roe JH. 2000. H_2O_2-sensitive Fur-like repressor CatR regulating the major catalase gene in *Streptomyces coelicolor*. J Biol Chem 275:38254–38260. https://doi.org/10.1074/jbc.M006079200.

43. Cremers CM, Jakob U. 2013. Oxidant sensing by reversible disulfide bond formation. J Biol Chem 288:26489–26496. https://doi.org/10.1074/jbc.R113.462929.

44. Helmann JD. 2014. Specificity of metal sensing: iron and manganese homeostasis in *Bacillus subtilis*. J Biol Chem 289:28112–28120. https://doi.org/10.1074/jbc.R114.587071.

45. Lisher JP, Giedroc DP. 2013. Manganese acquisition and homeostasis at the host-pathogen interface. Front Cell Infect Microbiol 3:91. https://doi.org/10.3389/fcimb.2013.00091.

46. Imlay JA. 2019. Where in the world do bacteria experience oxidative stress? Environ Microbiol 21:521–530. https://doi.org/10.1111/1462-2920.14445.

47. Aguirre JD, Culotta VC. 2012. Battles with iron: manganese in oxidative stress protection. J Biol Chem 287:13541–13548. https://doi.org/10.1074/jbc.R111.312181.

48. Turner AG, Ong CL, Gillen CM, Davies MR, West NP, McEwan AG, Walker MJ. 2015. Manganese homeostasis in group A *Streptococcus* is critical for resistance to oxidative stress and virulence. mBio 6:e00278-15. https://doi.org/10.1128/mBio.00278-15.

49. Rhodes DV, Crump KE, Makhlynets O, Snyder M, Ge X, Xu P, Stubbe J, Kitten T. 2014. Genetic characterization and role in virulence of the ribonucleotide reductases of *Streptococcus sanguinis*. J Biol Chem 289:6273–6287. https://doi.org/10.1074/jbc.M113.533620.

50. Xu Y, Itzek A, Kreth J. 2014. Comparison of genes required for H_2O_2 resistance in *Streptococcus gordonii* and *Streptococcus sanguinis*. Microbiology 160:2627–2638. https://doi.org/10.1099/mic.0.082156-0.

51. Marco S, Rullo R, Albino A, Masullo M, De Vendittis E, Amato M. 2013. The thioredoxin system in the dental caries pathogen *Streptococcus mutans* and the food-industry bacterium *Streptococcus thermophilus*. Biochimie 95:2145–2156. https://doi.org/10.1016/j.biochi.2013.08.008.

52. Tong H, Gao X, Dong X. 2003. *Streptococcus oligofermentans* sp. nov., a novel oral isolate from caries-free humans. Int J Syst Evol Microbiol 53:1101–1104. https://doi.org/10.1099/ijs.0.02493-0.

53. Lau PC, Sung CK, Lee JH, Morrison DA, Cvitkovitch DG. 2002. PCR ligation mutagenesis in transformable streptococci: application and efficiency. J Microbiol Methods 49:193–205. https://doi.org/10.1016/s0167-7012(01)00369-4.

54. Liu Y, Zeng L, Burne RA. 2009. AguR is required for induction of the *Streptococcus mutans* agmatine deiminase system by low pH and agmatine. Appl Environ Microbiol 75:2629–2637. https://doi.org/10.1128/AEM.02145-08.

55. LeBlanc DJ, Lee LN, Abu-Al-Jaibat A. 1992. Molecular, genetic, and functional analysis of the basic replicon of pVA380-1, a plasmid of oral streptococcal origin. Plasmid 28:130–145. https://doi.org/10.1016/0147-619X(92)90044-B.

56. Markvicheva KN, Bogdanova EA, Staroverov DB, Lukyanov S, Belousov VV. 2008. Imaging of intracellular hydrogen peroxide production with HyPer upon stimulation of HeLa cells with epidermal growth factor. Methods Mol Biol 476:79–86. https://doi.org/10.1007/978-1-59745-129-1_6.